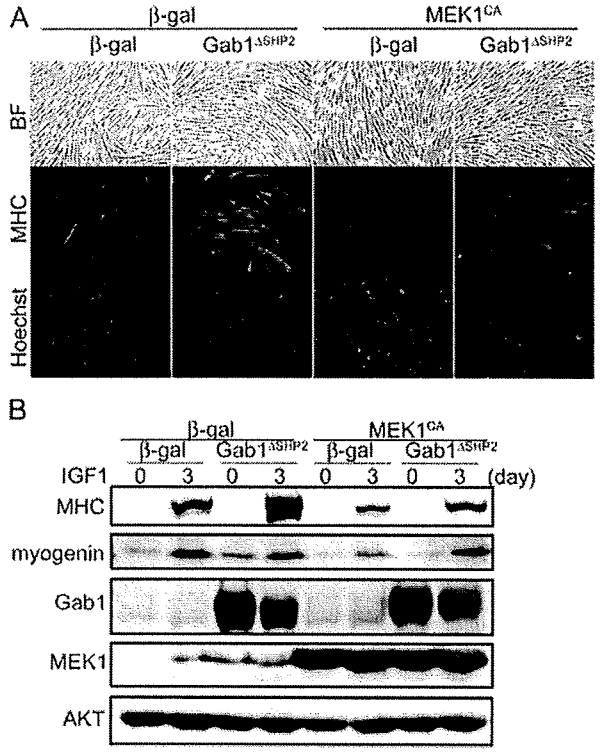

FIGURE 10. **Overexpression of constitutively active MEK1 abrogates the promoting effect of Gab1$^{\Delta SHP2}$ on myogenic differentiation in C2C12 cells.** *A*, C2C12 myoblasts were subjected to dual infection of adenovirus vectors expressing either β-gal or constitutively active MEK1 (MEK1^{CA}) with Gab1$^{\Delta SHP2}$. On the third day after myogenic induction, the cells were immunostained with anti-MHC antibody and post-stained with Hoechst 33342 nuclear dye. Overexpression of MEK1^{CA} in C2C12 significantly repressed the promoting effect of the overexpression of Gab1$^{\Delta SHP2}$ on IGF-I-induced myogenic differentiation. *B*, C2C12 myoblasts were subjected to dual infection of adenovirus vectors similar to *A*. The cell lysates were collected from 3.5-cm dishes and subjected to Western blot analysis. Dual overexpression of MEK1^{CA} with Gab1$^{\Delta SHP2}$ repressed the promoting effect of Gab1$^{\Delta SHP2}$ on the induction of MHC protein. Experiments were repeated three times with similar results.

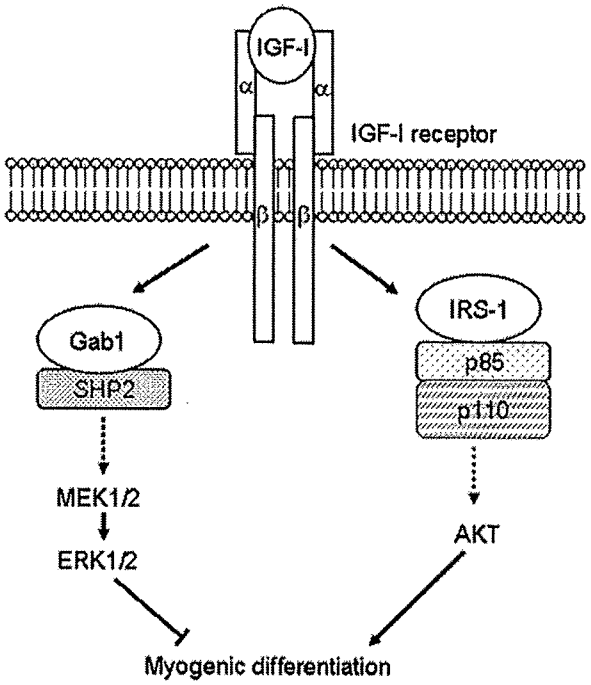

FIGURE 11. **Schematic models of the roles of Gab1 in IGF-I-dependent myogenic differentiation.** IGF-I induces tyrosine phosphorylation of Gab1 and subsequent association of Gab1 with SHP2. Gab1-SHP2 complex plays a critical role in activation of ERK1/2 in C2C12 myoblasts. Furthermore, Gab1-SHP2 complex negatively regulates myogenic differentiation via activation of MEK1/2-ERK1/2 pathway. On the other hand, IGF-I stimulation also induced tyrosine phosphorylation of IRS-I and subsequent association with p85 PI3K subunit. IRS-I-p85 complex formation has been reported to be indispensable for PI3K-AKT signaling, which might result in promotion of myogenic differentiation.

strates for the first time that Gab1 has an inhibitory role in IGF-I-induced myogenic differentiation through activating SHP2-MEK1/2-ERK1/2 signaling pathway.

IGF-I induced complex formation of Gab1 with SHP2 in C2C12 myoblasts. It has been reported that Gab1 undergoes dramatic tyrosine-dephosphorylation upon changing growth medium to differentiation medium containing 2% HS in C2C12 cells (42). This finding indicated that Gab1 might have a key role in myogenic differentiation. Recently, it has been reported that Gab1 itself is a substrate of SHP2 (39). Furthermore, it has been reported that phosphorylation of ERK1/2 decreases while phosphorylation of AKT increases during differentiation with either insulin or 2% HS (9). Therefore, tyrosine dephosphorylation of Gab1 and subsequent dissociation of SHP2 from dephosphorylated Gab1 might be essential steps for the diminution of ERK1/2 activity during myogenic differentiation.

The Gab1-SHP2 complex formation is indispensable for IGF-I-induced activation of ERK1/2. It has been reported that Gab1-SHP2 interaction has an essential role for ERK1/2 activation downstream of EGF family/ErbB receptor signaling or hepatocyte growth factor/c-Met signaling (20–23). Furthermore, the recent study creating liver-specific Gab1 knock-out mice also demonstrated that Gab1 is required for both insulin-elicited ERK1/2 activation and subsequent inhibition of IRS-1-PI3K-AKT signaling (34). Here, we demonstrated that overexpression of Gab1$^{\Delta SHP2}$, which is incapable of associating with SHP2, repressed IGF-I-dependent activation of ERK1/2 in C2C12 myoblasts. In a similar context, SHP2 itself has been reported to have crucial roles for ERK1/2 activation downstream of various growth factors, including IGF-I (24, 43–46). We also observed that overexpression of phosphatase-inactive SHP2 (SHP2$^{C/S}$) inhibited IGF-I-dependent activation of ERK1/2 in C2C12 myoblasts. These findings demonstrate that Gab1-SHP2 complex formation is requisite for both activation of SHP2 itself and ERK1/2 upon IGF-1 stimulation in C2C12 myoblasts. Because the mechanism how SHP2 regulates receptor tyrosine kinase-mediated ERK1/2 activation remains controversial (18, 19), further analyses are needed for uncovering the mechanism how Gab1-SHP2 complex regulates IGF-I-induced activation of ERK1/2.

The Gab1-SHP2 complex exerts an inhibitory effect on the IGF-I-induced myogenic differentiation through activation of ERK1/2. IGFs have been reported to stimulate both proliferation and differentiation of skeletal muscle cells in culture (3, 4). IGFs activate two major cytoplasmic signaling pathways, PI3K-AKT cascade and Raf-MEK1/2-ERK1/2 MAPK cascade. The former has been reported to have positive effects on myogenesis, and the latter MAPK-signaling cascade has been reported to have detrimental effects on the myogenic differentiation

induced by insulin or IGFs (3, 9, 10). SHP2 has been also reported to play an inhibitory role for myogenic differentiation in the presence of fibroblast growth factor 2 (FGF2) in C2C12 myoblasts partly in an ERK1/2-dependent manner (44). We found that IGF-I-induced myogenic differentiation was inhibited by overexpression of either Gab1^{WT} or Gab1$^{\Delta p85}$, but not by that of SHP2^{WT}. In addition, IGF-I-induced ERK1/2 activation in C2C12 myoblasts was enhanced by overexpression of either Gab1^{WT} or Gab1$^{\Delta p85}$, but not by that of SHP2^{WT}. SHP2 can be specifically activated through binding directly with tyrosine-phosphorylated docking proteins such as Gab1 or FRS2α (18), suggesting that a sufficient amount of Gab1 is required to fully activate SHP2 by binding with SHP2 and that an insufficient amount of endogenous Gab1 might be the major limiting factor in overexpressed SHP2^{WT}-mediated myogenic differentiation. Collectively, these data suggest that Gab1 is a crucial negative regulator for IGF-I-dependent myogenic differentiation through activation of the SHP2-MEK1/2-ERK1/2 signaling pathway (Fig. 10).

The migration of muscle progenitor cells into the limb anlage from somites is strongly impaired in Gab1-knock-out embryos similarly in c-Met-knock-out mice (32). Furthermore, it has been reported that the knock-in mice, which carry mutant Gab1 incapable of binding with SHP2, displayed quite similar defects in migration of muscle progenitor cells from somites into the limb anlage during embryogenesis as observed in Gab1-knock-out mice (29). In clear contrast, the knock-in mice, which carry mutant Gab1 incapable of binding either Grb2 or c-Met, did not show any defects in migration of muscle progenitor cells, suggesting the specific role of Gab1-SHP2 complex in the migration of muscle progenitor cells (29). These previous data coincide with our findings that Gab1-SHP2 interaction has an inhibitory effect on IGF-I-induced myogenic differentiation. Taken together, Gab1 might play a key role not only for inhibition of myogenesis but also for maintenance of the undifferentiated state of mesenchymal cells through activation of SHP2.

Although the PI3K-AKT signaling pathway is central to IGF-I-dependent signaling and myogenic differentiation, our data demonstrate that the diminution of ERK1/2 activity is a prerequisite for IGF-I-induced myogenesis. IGFs promote skeletal muscle differentiation through PI3K-AKT-dependent signaling pathway (3, 6, 7, 47–49). It has been reported that the activity of AKT increased during myogenic differentiation under cultivation in 2% HS or IGF-I-containing differentiation medium (9). We found that overexpression of Gab1$^{\Delta p85}$ in C2C12 myoblasts resulted in enhanced activation of AKT upon stimulation with IGF-I, compared with those overexpressing Gab1^{WT} or Gab1$^{\Delta SHP2}$. However, overexpression of Gab1$^{\Delta p85}$ did not enhance, but repressed IGF-I-induced myogenic differentiation to a similar extent to Gab1^{WT}. In clear contrast, overexpression of Gab1$^{\Delta SHP2}$ significantly enhanced IGF-I-induced myogenic differentiation compared with control. These findings indicate that myogenic differentiation requires the diminution of Gab1-SHP2-ERK1/2 signaling pathway prior to full activation of PI3K-AKT signaling pathway. It has been reported that the blockade of ERK1/2 signaling pathway enhances myogenic differentiation (3, 8–10). Inhibition of the ERK1/2 pathway has been reported to up-regulate Mirk/dyrk1B, a RhoA-dependent serine/threonine kinase that positively regulates skeletal muscle differentiation and inhibits apoptosis of myoblasts (50). Mirk/dyrk1B might be one of the candidate molecules through which ERK1/2 exerts an inhibitory effect on skeletal muscle differentiation.

In conclusion, the present study reveals that Gab1-SHP2 interaction exerts an inhibitory effect on IGF-I-dependent myogenic differentiation via activation of ERK1/2 signaling pathway.

Acknowledgments—We are grateful to S. Kawashima (Kobe University) for adenovirus vectors expressing dominant-negative MEK1 (MEK1^{DN}) and constitutively active MEK1 (MEK1^{CA}); T. Saito and S. Yamasaki (RIKEN Research Center for Allergy and Immunology) for Gab2$^{\Delta SHP2}$ cDNA; J. T. Pearson for his critical reading of this manuscript; Yuko Matsuura and Masako Suto for secretarial work; and Maki Yoshida, Y Mizushima, and Manami Sone for their technical assistance.

REFERENCES

1. Bach, L. A., Salemi, R., and Leeding, K. S. (1995) *Endocrinology* **136,** 5061–5069
2. Ewton, D. Z., Roof, S. L., Magri, K. A., McWade, F. J., and Florini, J. R. (1994) *J. Cell Physiol.* **161,** 277–284
3. Coolican, S. A., Samuel, D. S., Ewton, D. Z., McWade, F. J., and Florini, J. R. (1997) *J. Biol. Chem.* **272,** 6653–6662
4. Florini, J. R., Ewton, D. Z., and Coolican, S. A. (1996) *Endocr. Rev.* **17,** 481–517
5. White, M. F. (2003) *Science* **302,** 1710–1711
6. Kaliman, P., Vinals, F., Testar, X., Palacin, M., and Zorzano, A. (1996) *J. Biol. Chem.* **271,** 19146–19151
7. Kaliman, P., Canicio, J., Shepherd, P. R., Beeton, C. A., Testar, X., Palacin, M., and Zorzano, A. (1998) *Mol. Endocrinol.* **12,** 66–77
8. Bennett, A. M., and Tonks, N. K. (1997) *Science* **278,** 1288–1291
9. de Alvaro, C., Martinez, N., Rojas, J. M., and Lorenzo, M. (2005) *Mol. Biol. Cell* **16,** 4454–4461
10. Tortorella, L. L., Milasincic, D. J., and Pilch, P. F. (2001) *J. Biol. Chem.* **276,** 13709–13717
11. Gu, H., and Neel, B. G. (2003) *Trends Cell Biol.* **13,** 122–130
12. Nishida, K., and Hirano, T. (2003) *Cancer Sci.* **94,** 1029–1033
13. Holgado-Madruga, M., Emlet, D. R., Moscatello, D. K., Godwin, A. K., and Wong, A. J. (1996) *Nature* **379,** 560–564
14. Montagner, A., Yart, A., Dance, M., Perret, B., Salles, J. P., and Raynal, P. (2005) *J. Biol. Chem.* **280,** 5350–5360
15. Nishida, K., Yoshida, Y., Itoh, M., Fukada, T., Ohtani, T., Shirogane, T., Atsumi, T., Takahashi-Tezuka, M., Ishihara, K., Hibi, M., and Hirano, T. (1999) *Blood* **93,** 1809–1816
16. Takahashi-Tezuka, M., Yoshida, Y., Fukada, T., Ohtani, T., Yamanaka, Y., Nishida, K., Nakajima, K., Hibi, M., and Hirano, T. (1998) *Mol. Cell Biol.* **18,** 4109–4117
17. Weidner, K. M., Di Cesare, S., Sachs, M., Brinkmann, V., Behrens, J., and Birchmeier, W. (1996) *Nature* **384,** 173–176
18. Neel, B. G., Gu, H., and Pao, L. (2003) *Trends Biochem. Sci.* **28,** 284–293
19. Tiganis, T., and Bennett, A. M. (2007) *Biochem. J.* **402,** 1–15
20. Cunnick, J. M., Dorsey, J. F., Munoz-Antonia, T., Mei, L., and Wu, J. (2000) *J. Biol. Chem.* **275,** 13842–13848
21. Cunnick, J. M., Mei, L., Doupnik, C. A., and Wu, J. (2001) *J. Biol. Chem.* **276,** 24380–24387
22. Nakaoka, Y., Nishida, K., Fujio, Y., Izumi, M., Terai, K., Oshima, Y., Sugiyama, S., Matsuda, S., Koyasu, S., Yamauchi-Takihara, K., Hirano, T., Kawase, I., and Hirota, H. (2003) *Circ. Res.* **93,** 221–229
23. Schaeper, U., Gehring, N. H., Fuchs, K. P., Sachs, M., Kempkes, B., and Birchmeier, W. (2000) *J. Cell Biol.* **149,** 1419–1432

24. Cunnick, J. M., Meng, S., Ren, Y., Desponts, C., Wang, H. G., Djeu, J. Y., and Wu, J. (2002) *J. Biol. Chem.* **277,** 9498–9504
25. Dance, M., Montagner, A., Yart, A., Masri, B., Audigier, Y., Perret, B., Salles, J. P., and Raynal, P. (2006) *J. Biol. Chem.* **281,** 23285–23295
26. Jin, Z. G., Wong, C., Wu, J., and Berk, B. C. (2005) *J. Biol. Chem.* **280,** 12305–12309
27. Laramee, M., Chabot, C., Cloutier, M., Stenne, R., Holgado-Madruga, M., Wong, A. J., and Royal, I. (2007) *J. Biol. Chem.* **282,** 7758–7769
28. Mattoon, D. R., Lamothe, B., Lax, I., and Schlessinger, J. (2004) *BMC. Biol.* **2,** 24
29. Schaeper, U., Vogel, R., Chmielowiec, J., Huelsken, J., Rosario, M., and Birchmeier, W. (2007) *Proc. Natl. Acad. Sci. U. S. A.* **104,** 15376–15381
30. Rodrigues, G. A., Falasca, M., Zhang, Z., Ong, S. H., and Schlessinger, J. (2000) *Mol. Cell Biol.* **20,** 1448–1459
31. Itoh, M., Yoshida, Y., Nishida, K., Narimatsu, M., Hibi, M., and Hirano, T. (2000) *Mol. Cell Biol.* **20,** 3695–3704
32. Sachs, M., Brohmann, H., Zechner, D., Muller, T., Hulsken, J., Walther, I., Schaeper, U., Birchmeier, C., and Birchmeier, W. (2000) *J. Cell Biol.* **150,** 1375–1384
33. Nakaoka, Y., Nishida, K., Narimatsu, M., Kamiya, A., Minami, T., Sawa, H., Okawa, K., Fujio, Y., Koyama, T., Maeda, M., Sone, M., Yamasaki, S., Arai, Y., Koh, G. Y., Kodama, T., Hirota, H., Otsu, K., Hirano, T., and Mochizuki, N. (2007) *J. Clin. Invest.* **117,** 1771–1781
34. Bard-Chapeau, E. A., Hevener, A. L., Long, S., Zhang, E. E., Olefsky, J. M., and Feng, G. S. (2005) *Nat. Med.* **11,** 567–571
35. Yamasaki, S., Nishida, K., Yoshida, Y., Itoh, M., Hibi, M., and Hirano, T. (2003) *Oncogene* **22,** 1546–1556
36. Becker, T. C., Noel, R. J., Coats, W. S., Gomez-Foix, A. M., Alam, T., Gerard, R. D., and Newgard, C. B. (1994) *Methods Cell Biol.* **43,** 161–189
37. Ueyama, T., Kawashima, S., Sakoda, T., Rikitake, Y., Ishida, T., Kawai, M., Yamashita, T., Ishido, S., Hotta, H., and Yokoyama, M. (2000) *J. Mol. Cell Cardiol.* **32,** 947–960
38. Sarbassov, D. D., and Peterson, C. A. (1998) *Mol. Endocrinol.* **12,** 1870–1878
39. Zhang, S. Q., Tsiaras, W. G., Araki, T., Wen, G., Minichiello, L., Klein, R., and Neel, B. G. (2002) *Mol. Cell Biol.* **22,** 4062–4072
40. Meng, S., Chen, Z., Munoz-Antonia, T., and Wu, J. (2005) *Biochem. J.* **391,** 143–151
41. Yamasaki, S., Nishida, K., Hibi, M., Sakuma, M., Shiina, R., Takeuchi, A., Ohnishi, H., Hirano, T., and Saito, T. (2001) *J. Biol. Chem.* **276,** 45175–45183
42. Kontaridis, M. I., Liu, X., Zhang, L., and Bennett, A. M. (2001) *J. Cell Sci.* **114,** 2187–2198
43. Ivins, Z. C., Kontaridis, M. I., Fornaro, M., Feng, G. S., and Bennett, A. M. (2004) *J. Cell Physiol.* **199,** 227–236
44. Kontaridis, M. I., Liu, X., Zhang, L., and Bennett, A. M. (2002) *Mol. Cell Biol.* **22,** 3875–3891
45. Shi, Z. Q., Yu, D. H., Park, M., Marshall, M., and Feng, G. S. (2000) *Mol. Cell Biol.* **20,** 1526–1536
46. Shi, Z. Q., Lu, W., and Feng, G. S. (1998) *J. Biol. Chem.* **273,** 4904–4908
47. Jiang, B. H., Zheng, J. Z., Aoki, M., and Vogt, P. K. (2000) *Proc. Natl. Acad. Sci. U. S. A.* **97,** 1749–1753
48. Jiang, B. H., Zheng, J. Z., and Vogt, P. K. (1998) *Proc. Natl. Acad. Sci. U. S. A.* **95,** 14179–14183
49. Jiang, B. H., Aoki, M., Zheng, J. Z., Li, J., and Vogt, P. K. (1999) *Proc. Natl. Acad. Sci. U. S. A.* **96,** 2077–2081
50. Deng, X., Ewton, D. Z., Pawlikowski, B., Maimone, M., and Friedman, E. (2003) *J. Biol. Chem.* **278,** 41347–41354

Exercise-Induced Changes of Functional Mitral Regurgitation in Asymptomatic or Mildly Symptomatic Patients With Idiopathic Dilated Cardiomyopathy

Tetsuhiro Yamano, MD, PhD[a], Satoshi Nakatani, MD, PhD[a,*], Hideaki Kanzaki, MD[a], Norihisa Toh, MD[a], Makoto Amaki, MD[a], Jun Tanaka, MD[a], Haruhiko Abe, MD[a], Takuya Hasegawa, MD[a], Takahisa Sawada, MD, PhD[b], Hiroaki Matsubara, MD, PhD[b], and Masafumi Kitakaze, MD, PhD[a]

It has remained unclear why functional mitral regurgitation (MR), even if it is of a mild degree, has prognostic importance in patients with idiopathic dilated cardiomyopathy (IDC). Exercise-induced changes in functional MR, which might be a clue to this question, have not been fully clarified. Thus, in this study, semisupine exercise echocardiography was performed on 32 asymptomatic or mildly symptomatic patients with IDC (29 men, mean age 45 ± 14 years). The mean ejection fraction was 28 ± 10% (range 13% to 45%). The effective regurgitant orifice (ERO) area of MR was measured, as well as echocardiographic parameters including mitral valve geometry. ERO at rest was associated best with systolic mitral tenting area (r_S = 0.85, p <0.001). Functional MR did not newly appear during exercise in 9 subjects without MR at rest. In the remaining 23 subjects with functional MR at rest, all showed exacerbations of MR, with a median ERO of 10.5 mm^2 (interquartile range 6.3 to 16.5) to 18.7 mm^2 (interquartile range 9.5 to 29.3) (p <0.001). An increase in ERO was correlated best with the enlargement of tenting area (r_S = 0.90, p <0.001) and was the strongest independent determinant of exercise duration (β = −0.55, p = 0.002, multiple R^2 = 0.46). In conclusion, functional MR complicated with IDC was significantly exacerbated during exercise, with mitral valve deformation, which was strongly related to exercise intolerance; thus, the clinical impact of functional MR in patients with IDC could be more serious than can be expected by its degree at rest. **(Am J Cardiol 2008;102:481–485)**

It has not yet been fully clarified why even mild functional mitral regurgitation (MR) is an independent predictor of reduced survival in patients with idiopathic dilated cardiomyopathy (IDC).[1,2] Some studies have reported increases in functional MR with exercise,[3–6] which might be a clue to solving this question. However, these previous studies were limited to patients with left ventricular (LV) systolic dysfunction caused by ischemic heart disease. Changes in LV volume and the ejection fraction (EF) in response to exercise also might contribute to functional MR changes,[7] which should be different between patients with IDC and those with previous myocardial infarctions, from the viewpoint of neurohumoral responsiveness as well as regional LV function.[8,9] Thus, it is unknown whether mild functional MR in IDC changes during exercise. To clarify these issues, we investigated patients with IDC using exercise echocardiography.

Methods

We prospectively studied consecutive patients with IDC who were admitted to our institution for the further treatment of chronic heart failure or scrutiny for LV dysfunction from June 2005 to October 2006. They were all diagnosed with IDC, with echocardiographic LV diastolic internal dimensions >58 mm and EFs <50%, in the absence of angiographic coronary artery stenosis >50% and other specific cardiomyopathies. Inclusion criteria were (1) capability to perform an exercise test, (2) adequate echocardiographic images, and (3) normal sinus rhythm. Patients with structural mitral valve disease and those with uncontrollable ventricular arrhythmia were excluded. Finally, our study subjects consisted of 32 patients (29 men; mean age 45 ± 14 years; mean EF 28 ± 10%, range 13 to 45). Nine were in New York Heart Association functional class I and 23 were in class II. No patient was completely sedentary, and no one was engaged in regular exercise. Medical treatment included diuretics in 23 patients (72%), digitalis in 15 (47%), angiotensin-converting enzyme inhibitors or angiotensin II receptor blockers in 24 (75%), and β blockers in 27 (84%). All subjects gave written informed consent to the study protocol, which was approved by the institutional ethics committee.

A symptom-limited graded exercise test was performed in the semisupine position using a recumbent bicycle (Angio ergometer with Imaging Table; Lode BV, Groningen, The Netherlands). No cardiovascular drugs were discontin-

[a]Cardiovascular Division of Medicine, National Cardiovascular Center, Suita; and [b]Department of Cardiovascular Medicine, Kyoto Prefectural University of Medicine, Kyoto, Japan. Manuscript received January 9, 2008; revised manuscript received and accepted March 24, 2008.

*Corresponding author: Tel: 81-6-6833-5012; fax: 81-6-6872-7486.
E-mail address: nakatas@hsp.ncvc.go.jp (S. Nakatani).

0002-9149/08/$ – see front matter © 2008 Elsevier Inc. All rights reserved.
doi:10.1016/j.amjcard.2008.03.086

Table 1
Measurements at rest and Spearman's rank correlation coefficients (r_S) with effective regurgitant orifice at rest

Variable	Measurement at Rest	Correlation of ERO at Rest	
		r_S	p Value
Hemodynamic data			
Heart rate (beats/min)	68 ± 11	0.30	0.10
Systolic blood pressure (mm Hg)	114 ± 21	−0.58	<0.001
Diastolic blood pressure (mm Hg)	65 ± 12	−0.48	0.006
QRS duration (ms)	99 ± 25	0.43	0.01
ERO (mm^2)	6.5 (0.0–14.2)	—	—
Global LV remodeling			
End-diastolic volume index (ml/m^2)	118 (84–155)	0.73	<0.001
End-systolic volume index (ml/m^2)	86 (54–111)	0.74	<0.001
Diastolic sphericity index	1.80 (1.51–1.95)	−0.66	<0.001
Systolic sphericity index	1.87 (1.56–1.99)	−0.69	<0.001
EF (%)	28 ± 10	−0.56	0.001
Mitral valve deformation			
Tenting area (cm^2)	2.4 ± 0.8	0.85	<0.001
Coaptation height (cm)	1.1 ± 0.3	0.64	<0.001
Diastolic annular area (cm^2)	9.2 (8.5–10.7)	0.50	0.003
Systolic annular area (cm^2)	7.7 (7.4–8.9)	0.55	0.001
Annular contraction (%)	15 (12–17)	−0.23	0.21

Data were obtained from the entire cohort (n = 32) and are expressed as mean ± SD or as median (interquartile range).

ued before the exercise test. The workload was increased every 2 minutes by 25 W from an initial workload of 25 W, as previously described.[4,5] A standard 12-lead electrocardiogram was recorded before the exercise test. The electrocardiographic monitor was observed continuously, and blood pressure was recorded every 2 minutes. Echocardiograms were recorded using a standard ultrasound system (Toshiba SSA-770A; Toshiba Corporation, Tokyo, Japan). Quantitation of MR was performed using an effective regurgitant orifice (ERO) area from the proximal isovelocity surface area method, and the largest radius of the proximal isovelocity surface area, usually in early or late systole, was selected for analyses.[10] LV volume indexes as well as the EF were measured by the biplane modified Simpson's disk method, and the LV dimensionless sphericity index (the ratio of length to width) was also obtained.[11] Mitral annular area was calculated using an ellipsoid assumption, and its contraction was obtained.[11] From the parasternal long-axis view at mid-systole, the mitral tenting area was measured as the area enclosed between the annular plane and the mitral leaflets, and the coaptation height was the distance between the annular plane and leaflet coaptation.[11] For all measurements, ≥3 cardiac cycles were averaged.

Data are expressed as mean ± SD or median (interquartile range). Differences were tested for significance using Student's *t* test, the Mann-Whitney's U test, the paired Student's *t* test, or Wilcoxon's signed-rank test, as appropriate. Spearman's rank correlation coefficient (r_S) was used to study correlations with ERO. To determine the independent contributors to exercise duration, stepwise forward multiple linear regression analysis was performed, and the standardized coefficient (β) is shown. Interobserver variability was tested in 10 randomly selected subjects. A p value <0.05 was considered significant. All statistical analyses were performed using SPSS for Windows version 11.0J (SPSS Japan, Inc., Tokyo, Japan).

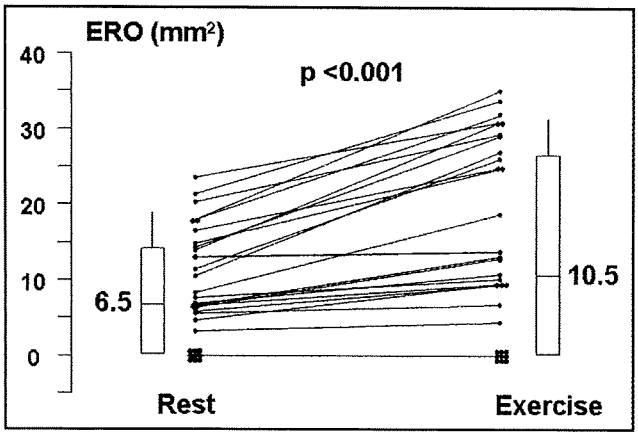

Figure 1. ERO of functional MR at rest and peak exercise in all subjects.

Results

The measurements at rest in the entire cohort and their correlations with ERO at rest are listed in Table 1. Functional MR was recognized in 23 subjects (72%; ERO range 2.4 to 23.6 mm^2), and 20 showed less than mild MR (ERO <20 mm^2).

ERO during exercise was significantly increased to 10.5 mm^2 (0 to 26.7) from the value at rest of 6.5 mm^2 (0 to 14.2) (p <0.001; Figure 1). In all subjects with functional MR at rest, MR was exacerbated to various degrees (ERO range 0.1 to 17.0 mm^2; Figure 2). However, functional MR did not newly appear during exercise in 9 subjects without MR at rest. Consequently, we performed the following analyses in 23 subjects with functional MR.

The measurements at rest and during exercise in subjects with functional MR are listed in Table 2. The mitral tenting area and coaptation height were increased in all subjects. Of the rest parameters and their changes, the correlations with increases in ERO are listed in Table 3. The strongest correlation was recognized with enlargement of systolic tenting area, and a significant association was also observed with ERO at rest (Figure 3). There was no statistically significant difference in ERO increases depending on medications (data not shown).

Fifteen subjects (65%) stopped exercise because of dyspnea and 8 (35%) because of fatigue. Heart rate, the EF, and ERO at rest and their changes, as well as QRS duration, gender, and age, were included in the multivariate model. The analysis showed the exercise-induced increase in ERO to be the strongest independent determinant (β = −0.55, p = 0.002) of exercise duration, followed by the EF measured at rest (β = 0.41, p = 0.02; multiple R^2 = 0.46, p = 0.001).

Linear regression analyses of the variables obtained by the 2 observers showed regression slopes near 1.0 for ERO and tenting area at rest and during exercise (r = 0.98 and

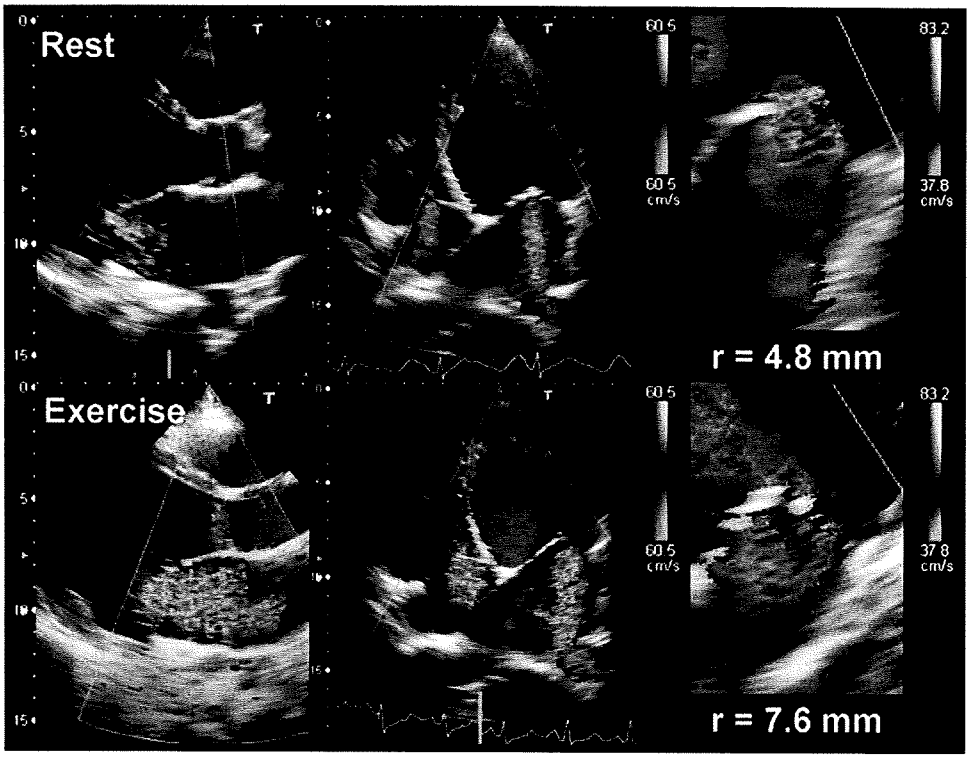

Figure 2. Color Doppler echocardiograms of a patient who showed a large increase in functional MR during exercise. These images reveal an obvious increase in MR by exercise. The radius of the proximal isovelocity surface area (r) was increased from 4.8 to 7.6 mm *(right)* and the ERO from 14.2 to 29.1 mm^2.

Table 2
Measurements at rest and during exercise in subjects with functional mitral regurgitation

Variable	Value at Rest	Exercise Value	p Value
Hemodynamic data			
Heart rate (beats/min)	72 (60–81)	110 (102–128)	<0.001
Systolic blood pressure (mm Hg)	106 ± 17	136 ± 20	<0.001
Diastolic blood pressure (mm Hg)	61 ± 11	67 ± 17	0.18
QRS duration (ms)	103 ± 26	—	—
ERO (mm^2)	10.5 (6.3–16.5)	18.7 (9.5–29.3)	<0.001
Global LV remodeling			
End-diastolic volume index (ml/m^2)	147 ± 53	151 ± 57	0.05
End-systolic volume index (ml/m^2)	114 ± 50	113 ± 51	0.21
Diastolic sphericity index	1.67 (1.44–1.94)	1.51 (1.37–1.87)	0.003
Systolic sphericity index	1.65 (1.50–1.94)	1.64 (1.45–1.90)	0.03
EF (%)	24 ± 7	27 ± 7	<0.001
Mitral valve deformation			
Tenting area (cm^2)	2.7 ± 0.6	3.5 ± 1.0	<0.001
Coaptation height (cm)	1.2 ± 0.3	1.5 ± 0.4	<0.001
Diastolic annular area (cm^2)	9.7 (9.0–11.6)	10.1 (9.5–11.7)	0.02
Systolic annular area (cm^2)	8.3 (7.5–9.4)	8.4 (8.0–9.7)	0.001
Annular contraction (%)	15 (12–17)	16 (12–20)	0.48
Exercise duration (min)		5.9 ± 2.4	—

Data were obtained from the subjects with functional MR (n = 23) and are expressed as mean ± SD or as median (interquartile range).

Table 3
Spearman's rank correlation coefficients (r_s) with exercise-induced changes in effective regurgitant orifice

Variable	Value at Rest		Exercise-Rest Value	
	r_s	p Value	r_s	p Value
Hemodynamic data				
Heart rate	−0.06	0.79	−0.26	0.23
Systolic blood pressure	−0.12	0.58	0.12	0.58
Diastolic blood pressure	−0.04	0.87	0.08	0.72
QRS duration	0.50	0.02	—	—
ERO	0.64	0.001	—	—
Global LV remodeling				
End-diastolic volume index	0.28	0.19	0.20	0.36
End-systolic volume index	0.24	0.28	−0.10	0.66
Diastolic sphericity index	−0.54	0.008	−0.15	0.50
Systolic sphericity index	−0.52	0.01	−0.39	0.07
EF	−0.06	0.78	0.27	0.21
Mitral valve deformation				
Tenting area	0.49	0.02	0.90	<0.001
Coaptation height	0.20	0.35	0.62	0.001
Diastolic annular area	0.32	0.14	0.15	0.49
Systolic annular area	0.42	0.05	0.30	0.17
Annular contraction	−0.10	0.65	0.01	0.95

Data were obtained from the subjects with functional MR (n = 23).

0.99, respectively, for ERO; r = 0.99 and 0.97, respectively, for tenting area). Bland-Altman analyses showed no significant biases (mean differences 0.8 ± 1.4 and 1.3 ± 1.7 mm^2 and 0.0 ± 0.1 and 0.0 ± 0.3 cm^2, respectively).

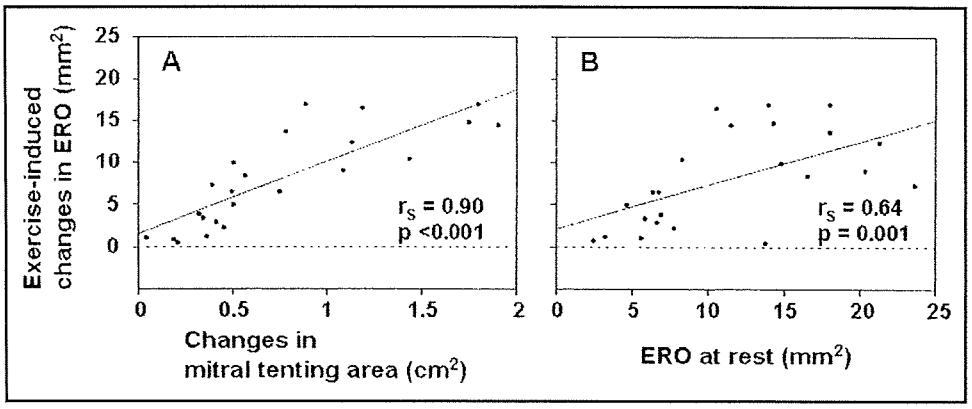

Figure 3. The correlation of the exercise-induced changes in ERO with those in mitral tenting area *(A)* and ERO at rest *(B)*.

Discussion

In the present study, functional MR in patients with IDC was significantly exacerbated during exercise, which was strongly related to their exercise intolerance. Thus, the clinical impact of functional MR complicated with IDC could be more serious than can be expected by its degree at rest. Patients with IDC who have functional MR should be carefully observed, even if MR is of a mild degree at rest.

Mitral tenting area was the strongest determinant of ERO at rest in patients with IDC, consistent with a previous study.[11] Besides, ERO was also associated with the EF, as well as LV volume indexes and mitral annular area. Considering these results, the mechanisms of functional MR in patients with IDC are as follows. The more severe LV systolic dysfunction, the more the LV cavity is dilated. LV dilatation leads to a large tenting area by displacement of the papillary muscles and mitral annular expansion, and LV systolic dysfunction decreases the closing force of the mitral leaflets; these 2 factors in tandem should aggravate functional MR.[12]

Enlargement of tenting area was found to be the strongest determinant of ERO exacerbation. Thus, in patients with IDC and previous myocardial infarctions, the exercise-induced changes in functional MR relate more strongly to the changes in mitral valve deformation than to those in global LV parameters.[5,6] In our series, the increases in ERO were significantly associated with the LV sphericity index at rest. Also, the sphericity index was significantly decreased, indicating that the shape of the left ventricle became more spherical during exercise. The LV sphericity change could increase mitral tenting area through excessive leaflet tethering, resulting in the exacerbation of functional MR.[6,13] However, considering the rough relations of the increases in ERO with changes in the sphericity index, the enlargement of tenting area could be multifactorial; other components such as alteration of localized bulging and systolic transmitral pressure should be considered.[7]

Differently from our results, previous studies have shown that there was no correlation between the exercise-induced changes in functional MR and its severity at rest.[5,6] This discrepancy may be related to the difference of study subjects, because those in the previous studies had previous myocardial infarctions. The regional wall motion abnormality induced by myocardial ischemia might relate to excessive exacerbation of functional MR,[3] and even subclinical ischemia presumably can cause wall motion abnormalities.[14] This also could cause the appearance of MR only during exercise,[15] whereas in the present study, functional MR did not newly appear during exercise in subjects without MR at rest. Moreover, contractile improvement of viable myocardium in the inferior region may lead functional MR to decrease in patients with previous myocardial infarctions.[5,6] However, we found no subjects showing decreases in MR during exercise in the present study. Therefore, it was considered that entire LV contractile augmentation of a mild degree could not decrease functional MR during exercise in most patients with IDC.

We had a small number of subjects, limited to asymptomatic or mildly symptomatic patients, because we included only patients who could perform exercise safely. Further study including more severely symptomatic patients could clarify if percutaneous or surgical interventions would be indicative for patients who show significant exacerbations of functional MR despite MR being of a mild degree at rest.[16,17] Clinical follow-up is also needed to confirm a prognostic value in exercise echocardiography for patients with IDC, as already demonstrated in pharmacologic stress echocardiography.[18]

The main limitation of our study is that we did not evaluate LV dyssynchrony using tissue Doppler imaging. D'Andrea et al[16] recently reported that increases in functional MR were independently associated with those in LV dyssynchrony measured by tissue Doppler imaging. In our study, patients with wide QRS durations tended to have large EROs at rest and large increases in ERO (Tables 1 and 3). A novel approach known as speckle-tracking imaging would make it possible to quantify LV dyssynchrony from routine 2-dimensional echocardiography.[19] A further study will be required to investigate the impact of LV dyssynchrony on exercise-induced exacerbation of functional MR. We could not apply the quantitative Doppler method because of its technical difficulties during exercise; however, the feasibility of the proximal isovelocity surface area method has been already proved, even during exercise.[10] Additionally, although there was no statistically difference in ERO changes depending on medications, we could not fully assess the impact of medications.

Acknowledgments: We thank Nobuo Shirahashi (Department of Preventive Medicine and Environmental Health, Osaka City University Graduate Medical School, Osaka, Japan) for valuable statistical advice.

1. Trichon BH, Felker GM, Shaw LK, Cabell CH, O'Connor CM. Relation of frequency and severity of mitral regurgitation to survival among patients with left ventricular systolic dysfunction and heart failure. *Am J Cardiol* 2003;91:538–543.
2. Blondheim DS, Jacobs LE, Kotler MN, Costacurta GA, Parry WR. Dilated cardiomyopathy with mitral regurgitation: decreased survival despite a low frequency of left ventricular thrombus. *Am Heart J* 1991;122:763–771.
3. Peteiro J, Bendayan I, Mariñas J, Campos R, Bouzas B, Castro-Beiras A. Prognostic value of mitral regurgitation assessment during exercise echocardiography in patients with left ventricular dysfunction: a follow-up study of 1.7 ± 1.5 years. *Eur J Echocardiogr* 2008;9:18–25.
4. Lancellotti P, Gérard PL, Piérard LA. Long-term outcome of patients with heart failure and dynamic functional mitral regurgitation. *Eur Heart J* 2005;26:1528–1532.
5. Lancellotti P, Lebrun F, Piérard LA. Determinants of exercise-induced changes in mitral regurgitation in patients with coronary artery disease and left ventricular dysfunction. *J Am Coll Cardiol* 2003;42:1921–1928.
6. Giga V, Ostojic M, Vujisic-Tesic B, Djordjevic-Dikic A, Stepanovic J, Beleslin B, Petrovic M, Nedeljkovic M, Nedeljkovic I, Milic N. Exercise-induced changes in mitral regurgitation in patients with prior myocardial infarction and left ventricular dysfunction: relation to mitral deformation and left ventricular function and shape. *Eur Heart J* 2005;26:1860–1865.
7. Levine RA. Dynamic mitral regurgitation—more than meets the eye. *N Engl J Med* 2004;351:1681–1684.
8. Deng MC, Brisse B, Erren M, Khurana C, Breithardt G, Scheld HH. Ischemic versus idiopathic cardiomyopathy: differing neurohumoral profiles despite comparable peak oxygen uptake. *Int J Cardiol* 1997;61:261–268.
9. Shen WF, Roubin GS, Hirasawa K, Choong CY, Hutton BF, Harris PJ, Fletcher PJ, Kelly DT. Left ventricular volume and ejection fraction response to exercise in chronic congestive heart failure: difference between dilated cardiomyopathy and previous myocardial infarction. *Am J Cardiol* 1985;55:1027–1031.
10. Lebrun F, Lancellotti P, Piérard LA. Quantitation of functional mitral regurgitation during bicycle exercise in patients with heart failure. *J Am Coll Cardiol* 2001;38:1685–1692.
11. Yiu SF, Enriquez-Sarano M, Tribouilloy C, Seward JB, Tajik AJ. Determinants of the degree of functional mitral regurgitation in patients with systolic left ventricular dysfunction: a quantitative clinical study. *Circulation* 2000;102:1400–1406.
12. He S, Fontaine AA, Schwammenthal E, Yoganathan AP, Levine RA. Integrated mechanism for functional mitral regurgitation: leaflet restriction versus coapting force: in vitro studies. *Circulation* 1997;96:1826–1834.
13. Lapu-Bula R, Robert A, Van Craeynest D, D'Hondt AM, Gerber BL, Pasquet A, Melin JA, De Kock M, Vanoverschelde JL. Contribution of exercise-induced mitral regurgitation to exercise stroke volume and exercise capacity in patients with left ventricular systolic dysfunction. *Circulation* 2002;106:1342–1348.
14. Lafitte S, Bordachar P, Lafitte M, Garrigue S, Reuter S, Reant P, Serri K, Lebouffos V, Berrhouet M, Jais P, et al. Dynamic ventricular dyssynchrony: an exercise-echocardiography study. *J Am Coll Cardiol* 2006;47:2253–2259.
15. Peteiro J, Freire E, Montserrat L, Castro-Beiras A. The effect of exercise on ischemic mitral regurgitation. *Chest* 1998;114:1075–1082.
16. D'Andrea A, Caso P, Cuomo S, Scarafile R, Salerno G, Limongelli G, Di Salvo G, Severino S, Ascione L, Calabrò P, et al. Effect of dynamic myocardial dyssynchrony on mitral regurgitation during supine bicycle exercise stress echocardiography in patients with idiopathic dilated cardiomyopathy and "narrow" QRS. *Eur Heart J* 2007;28:1004–1011.
17. Szalay ZA, Civelek A, Hohe S, Brunner-LaRocca HP, Klövekorn WP, Knez I, Vogt PR, Bauer EP. Mitral annuloplasty in patients with ischemic versus dilated cardiomyopathy. *Eur J Cardiothorac Surg* 2003;23:567–572.
18. Pratali L, Otasevic P, Neskovic A, Molinaro S, Picano E. Prognostic value of pharmacologic stress echocardiography in patients with idiopathic dilated cardiomyopathy: a prospective, head-to-head comparison between dipyridamole and dobutamine test. *J Card Fail* 2007;13:836–842.
19. Suffoletto MS, Dohi K, Cannesson M, Saba S, Gorcsan J III. Novel speckle-tracking radial strain from routine black-and-white echocardiographic images to quantify dyssynchrony and predict response to cardiac resynchronization therapy. *Circulation* 2006;113:960–968.

Biochemical and Biophysical Research Communications 370 (2008) 317–321

Contents lists available at ScienceDirect

Biochemical and Biophysical Research Communications

journal homepage: www.elsevier.com/locate/ybbrc

Higher mortality in heterozygous neuropilin-1 mice after cardiac pressure overload

Fei Li [a,c,1], Hui Zhao [a,1], Yulin Liao [a,b,*], Seiji Takashima [a], Yoshihiro Asano [a], Yasunori Shintani [a], Masatsugu Hori [a], Masafumi Kitakaze [b]

[a] Department of Cardiovascular Medicine, Osaka University Graduate School of Medicine, 2-2 Yamadaoka, Suita, Osaka 565-0871, Japan
[b] Department of Cardiovascular Medicine, National Cardiovascular Center, Osaka, Japan
[c] Department of Cardiovascular Medicine, Xijing Hospital, Fourth Military Medical University, Xi'an, China

ARTICLE INFO

Article history:
Received 17 March 2008
Available online 31 March 2008

Keywords:
Neuropilin-1
Heterozygote
Heart failure
Vascular endothelial growth factor
Cardiomyocytes
Mouse

ABSTRACT

We previously identified that neuropilin-1 (NP-1) was a co-receptor of vascular endothelial growth factor receptor 2 (VEGFR2) and confirmed that NP-1 knockout mice were embryonic lethal due to impairment of vascular development, while VEGF was reported to be involved in the progression of heart failure. However, it is unknown whether NP-1 has any influence on cardiac function, and it also remains poor understood concerning cardiac expression of NP-1 and its interaction with other VEGF receptors in the heart. Here, we first showed that NP-1 heterozygous mice had significantly higher mortality due to either acute or chronic heart failure in response to left ventricular pressure overload. We also observed that NP-1 mRNA and protein were expressed in both neonatal rat cardiomyocytes and adult murine heart. Furthermore, we found that NP-1 formed complexes with VEGFR1 and VEGFR2, respectively, in cardiomyocytes. These findings suggest that NP-1 should play beneficial role in heart failure.

Heart failure (HF) is the leading cause of death among patients with cardiovascular disease. Studies from our laboratory, as well as from others, have demonstrated that growth factors such as heparin-binding EGF-like growth factor [1], transforming growth factors [2] and vascular endothelial growth factor (VEGF) [3–5] were crucially involved in the progression of HF. By combination with its three receptors Flt-1 (VEGFR1), Flk-1/KDR (VEGFR2), and neuropilin-1 (NP-1), VEGF serves as an essential mediator of angiogenesis. We had identified that NP-1was a co-receptor of VEGFR2 [6] and confirmed that NP-1 knockout mice were embryonic lethal due to impairment of vascular development [7]. Interestingly, VEGF was demonstrated to play a protective role in the process of hypertrophic or diabetic cardiomyopathies [5,8,9]. It has been reported that VEGF blockage promoted the transition from compensatory cardiac hypertrophy to heart failure in response to pressure overload, while VEGF treatment improved cardiac angiogenesis and preserved myocardial contractile functions in pressure overloaded animals [10,11]. Furthermore, Inhibition of angiogenesis by a decoy VEGF receptor was demonstrated to promote the progression of HF [9,10]. Taken together, it is plausible to speculate that both VEGF and its receptors are important to preserve cardiac function. However, it remains completely unknown whether NP-1 also exerts any influence on HF, and little data is available on NP-1 expression in cardiomyocytes as well as its interaction with other receptors of VEGF in the heart.

We previously confirmed that NP-1 was essential for embryonic development and NP-1 knockout mice (NP-1(−/−)) died at E12.5–E13.5 with severe neural and vascular development defect, while no discernable abnormal vascular phenotype was observed in heterozygous NP-1 (NP-1 HE) mice [12,13]. Since change of VEGF receptors was believed to be associated with the progression of HF [9,10,14], we hypothesized that NP-1 HE mice would be susceptible to development of HF induced by pathological stress. To address this issue, we designed the present study to observe the survival curves of NP-1 HE mice and their wild-type (WT) littermates in response to transverse aortic constriction (TAC) and determine the cause of death. We also checked NP-1 expression in neonatal rat cardiomyocytes, fibroblasts and adult murine heart, and finally we investigated whether NP-1 is able to form complexes with Flt-1 and Flk-1in cardiomyocytes.

Materials and methods

Animal model. The heterozygous NP-1 mice (NP-1 HE) were generated as described elsewhere [7]. All procedures were performed in accordance with our institutional guidelines for animal research that conformed to the "Position of the

* Corresponding author. Address: Department of Cardiovascular Medicine, Osaka University Graduate School of Medicine, 2-2 Yamadaoka, Suita, Osaka 565-0871, Japan. Fax: +816 6879 3473.
E-mail address: liaoyulin@yahoo.com (Y. Liao).
[1] These authors contributed equally to this study.

0006-291X/$ - see front matter © 2008 Elsevier Inc. All rights reserved.
doi:10.1016/j.bbrc.2008.03.096

American Heart Association on Research Animal Use" adopted by the AHA on November 11, 1984. NP-1 HE mice and their WT littermates (male, 7–8 weeks old) were anesthetized with sodium pentobarbital (50 mg/kg, i.p.), and TAC was created as we described previously [15]. The occurrence of left ventricular pressure overload (increased systolic blood pressure) was confirmed with a Millar catheter inserted via the right carotid artery in three randomly selected mice from each group (NP-1 HE and WT groups, respectively) at 1 week after TAC. By daily observation of the mice and performing autopsy of the dead animals, we evaluated the survival rate and the cause of death. 36 mice (NP-1 HE, $n = 14$; WT, $n = 22$) were included and followed up for as long as more than 2 months.

Cell culture. Rat neonatal ventricular myocytes were isolated as described previously [15] and cultured in Dulbecco's modified Eagle's medium (DMEM; Sigma) supplemented with 10% fetal calf serum (FCS) (Equitech-Bio) which was changed to serum-free medium after 48 h. Cells were cultured under serum free condition for 24 h before being used. Cardiac fibroblasts obtained during the pre-plating step of the cardiomyocyte isolation procedure were maintained in 10% FCS-supplemented medium. After confluence, cells were trypsinized and passaged at 1:3 dilutions. The second passage fibroblasts were used.

RT-PCR. Total RNA of homogenized murine whole heart or cell lysates of cultured neonatal rat cardiomyocytes and fibroblasts were prepared using RNA-Bee isolation reagent (Tel-Test, Inc.) according to the protocol of the manufacturer. Reverse transcription-polymerase chain reaction (RT-PCR) was performed to generate cDNA templates from extracted RNA. cDNA template (1 μg) was then used for subsequent PCR amplification with primers targeting the genes of NP-1, flt-1, flk and GAPDH. PCR products were loaded onto a 1.5% agarose gel and electrophoresed at 100 V for 45 min. Gels were stained with ethidium bromide. GAPDH was used as internal control. The sequences of primers were as follows: mouse NP-1, sense: 5′-TATGACCGGCTGGAGATCTG-3′, antisense: 5′-TGTCCCTACAGCAGTAACGAA-3′; mouse flt-1, sense: 5′-CTGTCACCACAATCACTCCAA-3′, antisense: 5′-TCCTTCG GCTGGCATCTTTT-3′; mouse flk-1: sense: 5′- ATTGCCTGGTCAAACAGCTCA-3′, antisense: 5′-AGTGCCGACGAGGATAATGA-3′; rat NP-1, sense: 5′-TCCTGCGATTCGTT ACTGCT-3′, antisense: 5′- TCTTCTCATCTCCCAGGTCCA-3′; rat flt-1, sense: 5′-ACCATGCACCATAGCATCAGT-3′, antisense: 5′- CACCCTCATCCTCTTCTGTGA-3′; rat flk-1, sense: 5′-TATAAGAGCAAAGGGGCACG-3′, antisense:5′- ACACCAAAAGACCA CACACCA-3′.

Western blot and immunoprecipitation. For detecting the expression of NP-1, flk-1, and flt-1, SDS–PAGE was performed with 50 μg of protein extracted from rat cardiomyocytes and fibroblasts or 100 μg of protein from murine whole heart. Blots were incubated with antibodies: NP-1 C19, flt-1 C17, and flk-1 C1158 (Santa Cruz, USA). Immunoprecipitation was performed as described elsewhere [7]. Briefly, cells were grown in 6-well dishes, starved for 24 h and replaced with 2.0 ml binding buffer containing DMEM, 1 mg/ml BSA, and 1 μg/ml heparin. The cells were washed extensively with ice-cold phosphate-buffered saline (PBS) and lysed on ice with 300 μl of 30 mM MOPS, pH 7.0, 0.15 M NaCl, 1 mM Na_3VO_4, 5 mM NaF, 1 mM EDTA, 1% NP 40 and protease inhibitors. Cell lysates were incubated with anti-NP1, anti-flt-1 and anti-flt-1 antibodies at concentration of 1–2 μg/ml for 16 h at 4 °C and immune complexes were precipitated with protein G.

Statistical analysis. Results are reported as the mean ± SEM and two-tailed Student's *t*-test was used to compare the differences between groups. Survival analysis was performed using the Kaplan–Meier method. $P < 0.05$ was considered statistically significant.

Results and discussion

Higher mortality in NP-1 HE mice after TAC

Since NP-1 homozygous knockout mice are embryonic lethal, we used NP-1 HE mice to evaluate the role of NP-1 in HF. As we previously reported, NP-1 mRNA levels in NP-1 HE mice are less than one-half of wild-type mRNA levels [7]. During development up to adult, there was no cardiac phenotype was found in NP-1 HE mice. The results showed that systolic aortic blood pressure at baseline and 1 week after TAC was similar between WT and NP-1 HE mice (Fig. 1A), indicating similar pressure overload in the two TAC groups. By following up for two months, we found that the total mortality after TAC was markedly higher in NP-1 HE mice than in their WT littermates, the accumulated survival rates were 21% and 64% in NP-1 HE and WT mice, respectively, ($P = 0.0109$) (Fig. 1B), and the accumulated hazard of death was also significantly higher in NP-1 HE mice for the full follow-up period ($P = 0.0107$) (Fig. 1C). By daily observation of the mice and performing autopsy of the dead animals, we found that acute or chronic heart failure (CHF) was the cause of death, as indicated by the presence of pulmonary hemorrhage or congestion (Fig. 1D). The lung-to-body weight (LW/BW) ratio was usually higher than 13 mg/g (normal value is 5–6) and pleural effusion was common in mice that died of CHF. Additional analysis of acute mortality showed that nearly 50% of NP-1 HE mice versus 18% of WT mice died during the first week after TAC ($P = 0.0369$) (Fig. 1E). We further analyzed the chronic survival rate in the mice survived to 3 weeks. As a result, the mortality in the period of 21 to 60 days was 57% and 22% in NP-1 HE and WT groups, respectively ($P = 0.0108$) (Fig. 1F).

The above results are the first to show that partial deletion of NP-1 accelerates the development of lethal acute and chronic HF, suggesting an essential role of NP-1 in preserving heart function under pathological states. The higher incidence of lethal CHF in NP-1 HE mice may attribute to the disruption of coordinated cardiac hypertrophy and VEGF-mediated angiogenesis. It was reported that proportional capillary density with cardiac mass was necessary to preserve cardiac contractile function [8,9,16,17]. In TAC models, pressure overload initially induced adaptive hypertrophy with normal capillary density and cardiac contractile function; however, if the mechanical pressure sustained, the number of microvessel per cardiomyocyte decreased and systolic dysfunction developed. Inhibition of angiogenesis resulted in suppressed adaptive cardiac hypertrophy and deteriorated cardiac function [8]. It is highly believable that NP-1 plays a crucial role in VEGF medicated angiogenesis because inhibition of NP-1 attenuated murine retinal neovascularization stimulated by $VEGF_{165}$ [18]. And more persuasively, we previously demonstrated that serious angiogenesis defect occurred in NP-1 (−/−) mice [7]. Collectively, it is plausible that NP-1 contributes to preserving cardiac function through mediating VEGF-induced angiogenesis in pressure overload heart.

In term of the higher incidence of lethal acute HF in NP-1 HE mice, the mechanism of impaired angiogenesis may not be the case. We speculated that NP-1 might contribute to the VEGF mediated direct influence on cardiac function. In rat neonatal cardiomyocytes, VEGF was reported to directly enhance stretch-induced expression of connexin 43, an essential protein to form hemichannel and gap junctions which are necessary for electrical synchronization and normal systolic function in heart [19]. VEGF was also able to accelerate ventricular contractility in zebra fish and rat cardiomyocytes [4].

To clarify the precise mechanisms for the contribution of NP-1 disruption to lethal HF, substantial studies need to be undertaken. Here, we focused on two basic molecular issues: the expression of NP-1 and the relationship between NP-1 and other VEGF receptors in cardiomyocytes. Although NP-1 has been extensively addressed in endothelial cell, its molecular characteristics were rarely investigated in cardiomyocytes.

The expression of NP-1 in cardiomyocytes and fibroblasts

We observed that both mRNA and protein of NP-1 was expressed in rat neonatal cardiomyocytes, cardiac fibroblasts and adult murine heart (Fig. 2A–F), whereas Flt-1 and Flk-1 expressed in both neonatal rat cardiomyocytes (Fig. 2A and D) and adult murine whole heart (Fig. 2C and F) but were undetectable in neonatal rat cardiac fibroblasts (Fig. 2B and E).

Expression levels of NP-1 in fibroblasts were lower than in cardiomyocytes, suggesting that its expression in cardiomyocytes was not from contamination of fibroblast. Although NP-1 mRNA was reported to be expressed in human myocardium [6], to our knowledge, this study is the first to show both mRNA and protein of NP-1 expressed in neonatal animal cardiomyocytes and adult whole heart. Considering the co-existence of other VEGF receptors in cardiomyocytes, we speculated that NP-1 might exert some other role in myocardium besides angiogenesis, which need to be clarified in the future.

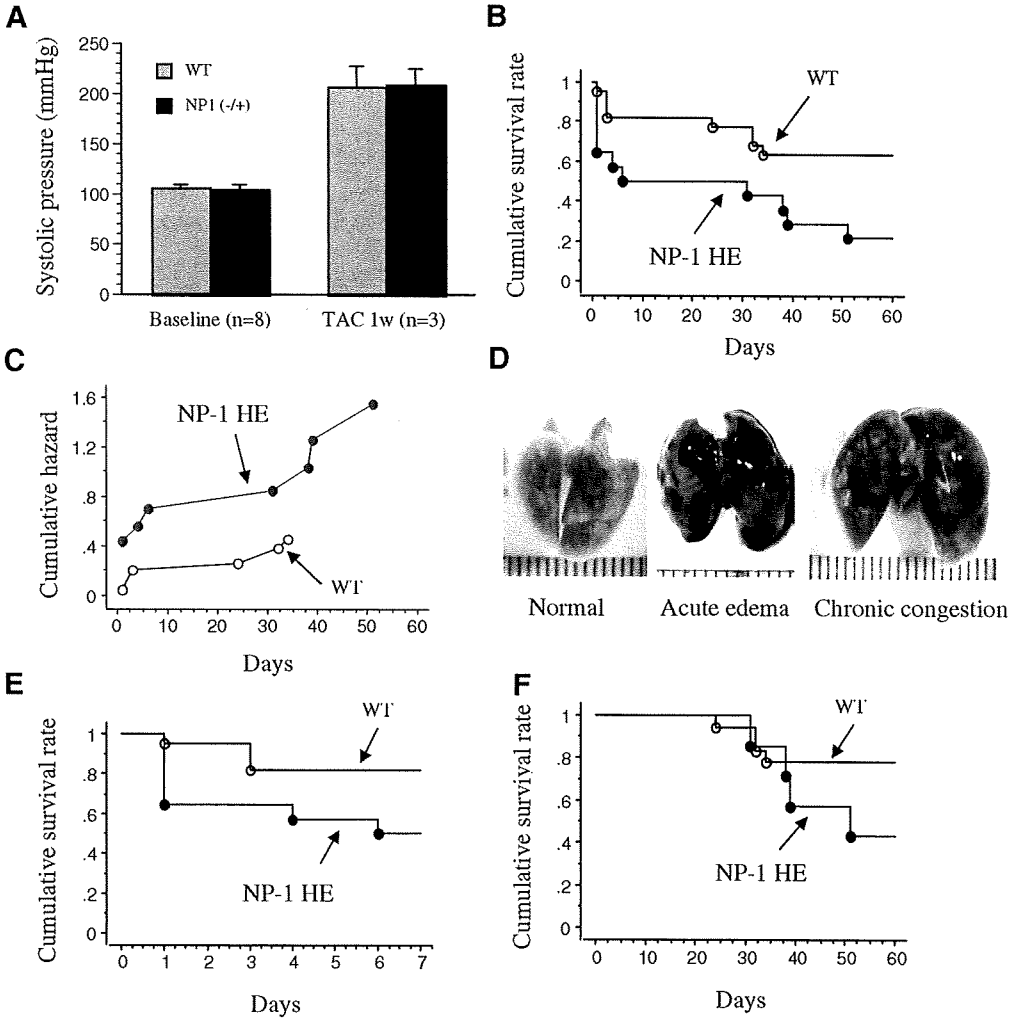

Fig. 1. Higher mortality rate in NP-1 HE mice in response to pressure overload. (A) No significant difference was found in systolic pressure before (baseline) and one week (1w) after transverse aortic constriction (TAC) operation in NP-1 HE and WT mice. (B) Kaplan–Meier cumulative survival analysis in NP-1 HE ($n = 14$) and WT ($n = 22$) mice after TAC. Lower cumulative survival rate was observed in NP-1 HE than in WT ones ($P = 0.0109$). (C) Cumulative hazard curve showed higher hazard in NP-1 HE mice than in WT ones ($P = 0.0107$). (D) Acute pulmonary hemorrhage or edema and chronic pulmonary congestion were observed in dead mice after TAC. (E) Kaplan–Meier curve within 7 days after TAC. Higher mortality rate occurred in NP-1 HE ($n = 14$) mice than in WT ($n = 22$) ones after TAC ($P = 0.0369$). (F) Kaplan–Meier curve in the mice survived to 3 weeks after TAC. Much higher mortality rate was observed in NP-1 HE ($n = 7$) mice than in WT littermate ($n = 18$) ($P = 0.0108$).

Complex formation of NP-1 and other two VEGF receptors in cardiomyocytes

In endothelial cells, NP-1 can associate with Flt-1 or Flk-1 and form complex by $VEGF_{165}$ stimulation [20]. To examine whether it is the case in cardiomyocytes, we used anti-NP-1 antibody to immunoprecipitate rat neonatal cardiomyocyte lysates and then performed immunoblot with antibodies of Flt-1, Flk-1, and VEGF, respectively, with or without VEGF pretreatment. The results show that Flt-1, Flk-1, and VEGF were detected in NP-1 immunoprecipitated products independent of VEGF pretreatment (Fig. 3A). To confirm the complex formation, we further immunoprecipitated cardiomyocyte lysates with anti-flt-1 and anti-flk-1 antibodies, respectively, and then immunoblotted with VEGF or NP-1 antibody. As shown in Fig. 3B, in both anti-Flt-1 and anti-Flk-1 immunoprecipitated products, NP-1 and VEGF were detected independent of VEGF pretreatment.

These findings revealed that NP-1 can form complexes with Flt-1 and Flk-1 in cardiomyocytes, providing the molecular basis that NP-1 might be involved in VEGF mediated influence on cardiomyocytes such as angiogenesis or myocytes contractility. Usually, it is recognized that exogenous $VEGF_{165}$ stimulation is necessary for NP-1 to bind Flt-1 and Flk-1, but in the present study, NP-1 combined with other two VEGF receptors independent of VEGF pretreatment. A reasonable interpretation is that cardiomyocytes can produce sufficient endogenous VEGF as we detected in this study to promote the combination of ligand and its receptors, and addition of exogenous VEGF could not further affect the binding efficiency.

In summary, in this study we first found that partial disruption of NP-1 significantly increased the incidence of both acute and chronic heart failure as well as the mortality after left ventricular pressure overload in mice, and we further confirmed the expression and complex formation of NP-1 and other two VEGF receptors in cardiomyocytes. These findings suggest that NP-1 play a pivotal role in preserving cardiac function in response to pressure overload and imply that NP-1 as well as VEGF and its other two receptors may be potential targets for heart failure therapy.

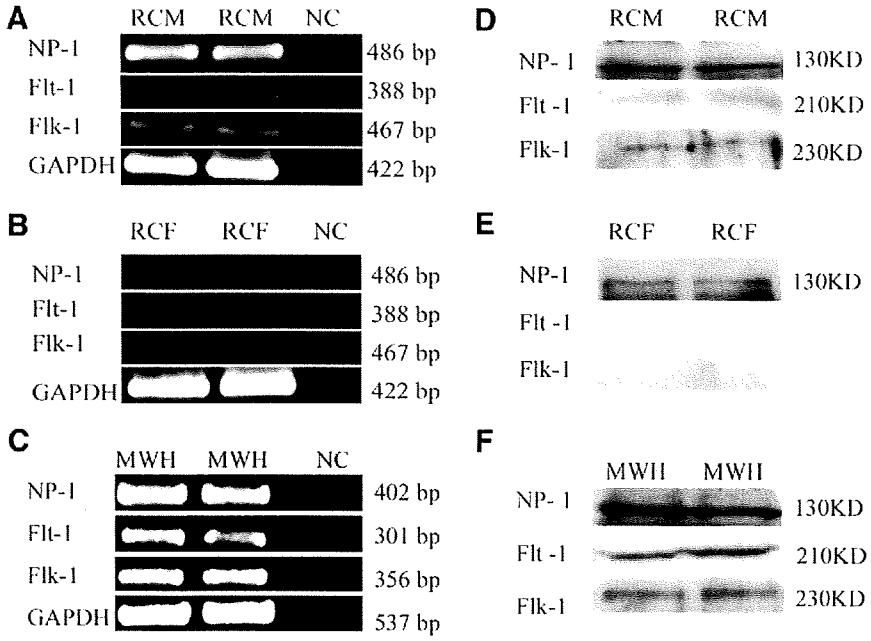

Fig. 2. The expression of VEGF receptors in rat cardiomyocytes (RCM), rat cardiac fibroblasts (RCF) and murine whole heart (MWH). (A–C) The mRNA levels of NP-1, Flt-1 and Flk-1 analyzed by RT-PCR. NC, negative control. (D–F) The protein expression of NP-1, Flt-1, and Flk-1 analyzed by Western blot.

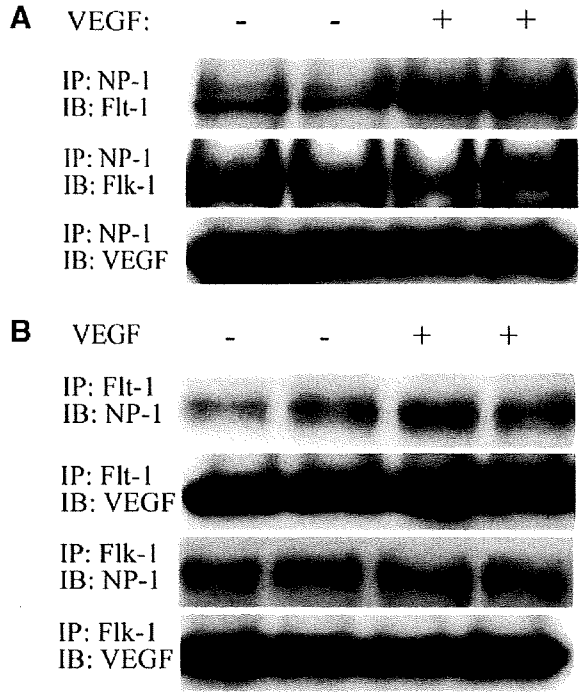

Fig. 3. NP-1 formed complexes with Flt-1 and Flk-1, respectively, in rat neonatal cardiomyocytes. Rat neonatal cardiomyocytes were incubated in the presence or absence of VEGF (20 ng/ml) for 30 min on ice and 7 min at 37 °C.(A) Cardiomyocyte lysates were immunoprecipitated with anti-NP 1 antibody and immunoblotted with anti-Flk-1, anti-Flt-1, and anti-VEGF antibodies, respectively. (B) Cardiomyocyte lysates were immunoprecipitated with anti-Flk-1 or anti-Flt-1 antibodies and immunoblotted with anti-NP-1 and anti-VEGF antibodies, respectively.

Acknowledgments

This work was supported by grants (H13-21seiki (seikatsu)-23) from the Japanese Ministry of Health, Labor and Welfare. Dr. Li was financial supported by The Japan–China Sasakawa Medical Fellowship 2007; Dr. Liao was supported by a grant from the Japan Society for the Promotion of Science (P05228).

References

[1] M. Asakura, M. Kitakaze, S. Takashima, Y. Liao, F. Ishikura, T. Yoshinaka, H. Ohmoto, K. Node, K. Yoshino, H. Ishiguro, H. Asanuma, S. Sanada, Y. Matsumura, H. Takeda, S. Beppu, M. Tada, M. Hori, S. Higashiyama, Cardiac hypertrophy is inhibited by antagonism of ADAM12 processing of HB-EGF: metalloproteinase inhibitors as a new therapy, Nat. Med. 8 (2002) 35–40.
[2] H.L. Li, C. Liu, G. de Couto, M. Ouzounian, M. Sun, A.B. Wang, Y. Huang, C.W. He, Y. Shi, X. Chen, M.P. Nghiem, Y. Liu, M. Chen, F. Dawood, M. Fukuoka, Y. Maekawa, L. Zhang, A. Leask, A.K. Ghosh, L.A. Kirshenbaum, P.P. Liu, Curcumin prevents and reverses murine cardiac hypertrophy, J. Clin. Invest. 118 (2008) 879–893.
[3] P. Carmeliet, Y.S. Ng, D. Nuyens, G. Theilmeier, K. Brusselmans, I. Cornelissen, E. Ehler, V.V. Kakkar, I. Stalmans, V. Mattot, J.C. Perriard, M. Dewerchin, W. Flameng, A. Nagy, F. Lupu, L. Moons, D. Collen, P.A. D'Amore, D.T. Shima, Impaired myocardial angiogenesis and ischemic cardiomyopathy in mice lacking the vascular endothelial growth factor isoforms VEGF164 and VEGF188, Nat. Med. 5 (1999) 495–502.
[4] W. Rottbauer, S. Just, G. Wessels, N. Trano, P. Most, H.A. Katus, M.C. Fishman, VEGF-PLCgamma1 pathway controls cardiac contractility in the embryonic heart, Genes Dev. 19 (2005) 1624–1634.
[5] Y.S. Yoon, S. Uchida, O. Masuo, M. Cejna, J.S. Park, H.C. Gwon, R. Kirchmair, F. Bahlman, D. Walter, C. Curry, A. Hanley, J.M. Isner, D.W. Losordo, Progressive attenuation of myocardial vascular endothelial growth factor expression is a seminal event in diabetic cardiomyopathy: restoration of microvascular homeostasis and recovery of cardiac function in diabetic cardiomyopathy after replenishment of local vascular endothelial growth factor, Circulation 111 (2005) 2073–2085.
[6] S. Soker, S. Takashima, H.Q. Miao, G. Neufeld, M. Klagsbrun, Neuropilin-1 is expressed by endothelial and tumor cells as an isoform-specific receptor for vascular endothelial growth factor, Cell 92 (1998) 735–745.
[7] S. Takashima, M. Kitakaze, M. Asakura, H. Asanuma, S. Sanada, F. Tashiro, H. Niwa, J. Miyazaki Ji, S. Hirota, Y. Kitamura, T. Kitsukawa, H. Fujisawa, M. Klagsbrun, M. Hori, Targeting of both mouse neuropilin-1 and neuropilin-2 genes severely impairs developmental yolk sac and embryonic angiogenesis, Proc. Natl. Acad. Sci. USA 99 (2002) 3657–3662.
[8] K. Walsh, I. Shiojima, Cardiac growth and angiogenesis coordinated by inter tissue interactions, J. Clin. Invest. 117 (2007) 3176–3179.
[9] I. Shiojima, K. Sato, Y. Izumiya, S. Schiekofer, M. Ito, R. Liao, W.S. Colucci, K. Walsh, Disruption of coordinated cardiac hypertrophy and angiogenesis contributes to the transition to heart failure, J. Clin. Invest. 115 (2005) 2108–2118.
[10] Y. Izumiya, I. Shiojima, K. Sato, D.B. Sawyer, W.S. Colucci, K. Walsh, Vascular endothelial growth factor blockade promotes the transition from

compensatory cardiac hypertrophy to failure in response to pressure overload, Hypertension 47 (2006) 887–893.
[11] I. Friehs, R. Barillas, N.V. Vasilyev, N. Roy, F.X. McGowan, P.J. del Nido, Vascular endothelial growth factor prevents apoptosis and preserves contractile function in hypertrophied infant heart, Circulation 114 (2006) I290–I295.
[12] T. Kawasaki, T. Kitsukawa, Y. Bekku, Y. Matsuda, M. Sanbo, T. Yagi, H. Fujisawa, A requirement for neuropilin-1 in embryonic vessel formation, Development 126 (1999) 4895–4902.
[13] T. Kitsukawa, M. Shimizu, M. Sanbo, T. Hirata, M. Taniguchi, Y. Bekku, T. Yagi, H. Fujisawa, Neuropilin–semaphorin III/D-mediated chemorepulsive signals play a crucial role in peripheral nerve projection in mice, Neuron 19 (1997) 995–1005.
[14] S. Fukuda, S. Kaga, L. Zhan, D. Bagchi, D.K. Das, A. Bertelli, N. Maulik, Resveratrol ameliorates myocardial damage by inducing vascular endothelial growth factor-angiogenesis and tyrosine kinase receptor Flk-1, Cell Biochem. Biophys. 44 (2006) 43–49.
[15] Y. Liao, M. Asakura, S. Takashima, H. Kato, Y. Asano, Y. Shintani, T. Minamino, H. Tomoike, M. Hori, M. Kitakaze, Amlodipine ameliorates myocardial hypertrophy by inhibiting EGFR phosphorylation, Biochem. Biophys. Res. Commun. 327 (2005) 1083–1087.
[16] M. Sano, T. Minamino, H. Toko, H. Miyauchi, M. Orimo, Y. Qin, H. Akazawa, K. Tateno, Y. Kayama, M. Harada, I. Shimizu, T. Asahara, H. Hamada, S. Tomita, J.D. Molkentin, Y. Zou, I. Komuro, p53-induced inhibition of Hif-1 causes cardiac dysfunction during pressure overload, Nature 446 (2007) 444–448.
[17] J. Heineke, M. Auger-Messier, J. Xu, T. Oka, M.A. Sargent, A. York, R. Klevitsky, S. Vaikunth, S.A. Duncan, B.J. Aronow, J. Robbins, T.M. Cromblehol, J.D. Molkentin, Cardiomyocyte GATA4 functions as a stress-responsive regulator of angiogenesis in the murine heart, J. Clin. Invest. 117 (2007) 3198–3210.
[18] H. Oh, H. Takagi, A. Otani, S. Koyama, S. Kemmochi, A. Uemura, Y. Honda, Selective induction of neuropilin-1 by vascular endothelial growth factor (VEGF): a mechanism contributing to VEGF-induced angiogenesis, Proc. Natl. Acad. Sci. USA 99 (2002) 383–388.
[19] R.C. Pimentel, K.A. Yamada, A.G. Kleber, J.E. Saffitz, Autocrine regulation of myocyte Cx43 expression by VEGF, Circ. Res. 90 (2002) 671–677.
[20] S. Soker, H.Q. Miao, M. Nomi, S. Takashima, M. Klagsbrun, VEGF165 mediates formation of complexes containing VEGFR-2 and neuropilin-1 that enhance VEGF165-receptor binding, J. Cell. Biochem. 85 (2002) 357–368.

Available online at www.sciencedirect.com
ScienceDirect
Biochemical and Biophysical Research Communications 365 (2008) 541–547
BBRC
www.elsevier.com/locate/ybbrc

Identification of a novel substrate for TNFα-induced kinase NUAK2

Hiroyuki Yamamoto [a], Seiji Takashima [b,c,*], Yasunori Shintani [b], Satoru Yamazaki [d], Osamu Seguchi [d], Atsushi Nakano [d], Shuichiro Higo [b], Hisakazu Kato [b], Yulin Liao [d], Yoshihiro Asano [b], Tetsuo Minamino [b], Yasushi Matsumura [a], Hiroshi Takeda [a], Masafumi Kitakaze [d]

[a] *Department of Medical Information Science, Osaka University Graduate School of Medicine, Suita, Osaka 565-0871, Japan*
[b] *Department of Cardiovascular Medicine, Osaka University Graduate School of Medicine, 2-2 Yamadaoka, Suita, Osaka 565-0871, Japan*
[c] *Health Care Center, Osaka University Graduate School of Medicine, Suita, Osaka 565-0871, Japan*
[d] *Department of Cardiovascular Medicine, National Cardiovascular Center, Suita, Osaka 565-8565, Japan*

Received 2 November 2007
Available online 20 November 2007

Abstract

TNFα has multiple important cellular functions both in normal cells and in tumor cells. To explore the role of TNFα, we identified NUAK family, SNF1-like kinase 2 (NUAK2), as a TNFα-induced kinase by gene chip analysis. NUAK2 is known to be induced by various cellular stresses and involved in cell mortality, however, its substrate has never been identified. We developed original protocol of de novo screening for kinase substrates using an in vitro kinase assay and high performance liquid chromatography (HPLC). Using this procedure, we identified myosin phosphatase target subunit 1 (MYPT1) as a specific substrate for NUAK2. MYPT1 was phosphorylated at another site(s) by NUAK2, other than known Rho-kinase phosphorylation sites (Thr696 or Thr853) responsible for inhibition of myosin phosphatase activity. These data suggests different phosphorylation and regulation of MYPT1 activity by NUAK2.

Keywords: NUAK family, SNF1-like kinase 2 (NUAK2); Myosin phosphatase target subunit 1 (MYPT1); TNFα; Myosin phosphatase; In vitro kinase assay

Tumor necrosis factor (TNFα) has multiple cellular functions both in normal cells and in tumor cells. TNFα not only induces apoptotic cell death but also enhances various gene expressions mediated by NFκB family transcriptional factors. Endothelial cells express TNFα receptors, and its NFκB-mediated signals induce various chemokine related molecules and cell adhesion molecules. These molecules enhance attachment of mononuclear cells and help these cells to enter into inflammatory tissues through endothelial cell barrier. TNFα also induces chemotactic molecules of endothelial cell, indicating that cell mobility induced by TNFα signal is mediated by as yet unidentified molecular mechanisms [1].

In the current study, we demonstrated that NUAK family, SNF1-like kinase 2 (NUAK2) was identified as a TNFα-induced kinase in endothelial cells by gene chip analysis. NUAK2 was originally identified in a PCR-based screen designed to identify a novel protein kinase [2]. Subsequent studies indicated that NUAK2 was induced by various cellular stresses such as ER stress, elevation of cellular AMP, hyperosmotic stress, and ultraviolet [3]. High expression of NUAK2 was also confirmed in various tumor cell lines [4], and overexpression of NUAK2 was reported to render tumor cell resistance under apoptotic stimuli. Such inductions and expressional mechanisms of NUAK2 have

* Corresponding author. Address: Department of Cardiovascular Medicine, Osaka University Graduate School of Medicine, 2-2 Yamadaoka, Suita, Osaka 565-0871, Japan. Fax: +81 6 8679 3473.
E-mail address: takasima@medone.med.osaka-u.ac.jp (S. Takashima).

0006-291X/$ - see front matter © 2007 Elsevier Inc. All rights reserved.
doi:10.1016/j.bbrc.2007.11.013

been well reported, however its substrate has never been identified.

Diverse effects of kinases in various tissues depend on specific substrates. To reveal the function of kinase it is essential to purify its substrate. Here, we identified myosin phosphatase target subunit 1 (MYPT1) as a specific substrate for NUAK2 using unique purification procedure. This method was designed to purify target substrates by combination of an in vitro kinase assay and high performance liquid chromatography (HPLC). NUAK2 phosphorylated MYPT1 at a distinct site(s) other than known Rho-kinase (ROCK) phosphorylation sites (Thr696 or Thr853) responsible for inhibition of myosin phosphatase activity, suggesting different phosphorylation and regulation of MYPT1 activity by NUAK2.

Materials and methods

Cell lines and reagents. Human umbilical vein endothelial cells (HUVECs) and human aortic smooth muscle cells (AoSMCs) were obtained from Clonetics. They were cultured in endothelial and smooth muscle cell medium (Clonetics) and used up to passage 5. HEK293T cells and HeLa cells were cultured in DMEM with 10% FBS. The following antibodies were purchased: anti-Flag (M2Ab; Sigma), anti-V5 (Invitrogen), anti-Myc (Invitrogen), anti-Tubulin (Cell Signaling), anti-NUAK2 (Abgent), anti-MYPT1 (BD Biosciences), anti-phospho-MYPT1 (Thr696) (Upstate Biotechnology), and anti-phospho-MYPT1 (Thr853) (CycLex). The following reagents were purchased: Trypsin (Promega), Lipofectamine 2000 (Invitrogen), Flag peptide (Sigma), and human recombinant TNFα (R&D Systems, Inc.).

cDNA microarray analysis. To determine the effect of TNFα on gene expression profile, we treated cultured HUVECs without or with TNFα (20 ng/ml) for 2 h, and then performed cDNA microarray studies. Total RNA was prepared from HUVECs using RNA-Bee-RNA Isolation Reagent (Tel-Test Inc.) according to the manufacturer's instructions. Microarray hybridization was performed in triplicate using Affymetrix Human Genome 133A gene chips (HG-U133A). After synthesizing double-stranded cDNA from the total RNA, an in vitro transcription reaction was done to produce biotin-labeled cRNA from cDNA, and the cRNA was fragmented before hybridization. Hybridization, probe washing, staining and probe array scanning were performed following the protocols provided by Affymetrix. Data were analyzed using Genespring 6 software [5]. Normalization was done by a combination of three steps: rewriting negative values as 0.01, normalizing to the 50th percentile per chip and normalizing to the median per gene. We filtered data using a combination of parameters such as signal confidence ('present' flag), fold change (>3), minimum acceptable signal intensity (average difference $\geqslant$50 in at least one of the two groups). Indicated gene accession numbers were derived from the GenBank database.

Northern blot analysis. Northern blot analysis was performed as previously described [6]. Briefly, total RNA was isolated and electrophoresed on 1% agarose gel containing 2.2 M formaldehyde, and transferred onto nylon membranes (Bio-Rad). The membranes were hybridized with ^{32}P-labeled fragments of human cDNA corresponding to nucleotides 1–1887 of NUAK2 cDNA. A BAS photoimaging system (Fuji) was used for detection.

Quantitative RT–PCR. Total RNA was extracted using RNA-Bee-RNA Isolation Reagent (Tel-Test Inc.). Then, 1 μg of total RNA was reverse-transcribed using Omniscript RT (Qiagen) according to the manufacturer's protocol. Quantitative RT-PCR was performed with TaqMan technology using the ABI Prism 7000 detection system (Applied Biosystems) according to the manufacturer's instructions. RT-PCR conditions were 2 min at 50 °C, 10 min at 95 °C, and 40 cycles of 15 s at 95 °C and 1 min at 60°C. Data were normalized to 18S ribosomal RNA or GAPDH level. Each sample was analyzed in duplicate and the experiments were replicated three times. For 18S ribosomal RNA, GAPDH and NUAK2, primers and probes were obtained using TaqMan Assays-on-Demand gene expression products (Applied Biosystems).

Cloning, plasmid construction, and mutagenesis. In this experiment, all construction was performed using the Gateway system (Invitrogen) according to the manufacturer's instructions. Human NUAK2 cDNA was isolated from HUVECs cDNA using the following sense and antisense primers: sense 5′ caccatggagtcgctggttttcg and antisense 5′ tcaggtgagctttgagcagaccc. With PCR primer designed to include stop codon of NUAK2, the amplified fragment was inserted into pENTR/D-TOPO (Invitrogen), named pENTR/NUAK2. To generate N-terminal Flag-tagged NUAK2 (Flag-NUAK2), Flag epitope (DYKDDDDK) was introduced into just before the N terminus of NUAK2 by PCR-based mutagenesis using pENTR/NUAK2 as a template. The NUAK2 constructs were recombined to mammalian expression vector, pcDNA3.1 vector (Invitrogen). We also generated N-terminal Myc-tagged NUAK2 (Myc-NUAK2) using the same protocol. cDNA encoding human MYPT1 was generated by RT-PCR with RNA from HUVECs. The mammalian expression vectors for MYPT1 were constructed using pENTR/D-TOPO (pENTR-MYPT1). To identify the binding site on MYPT1 for NUAK2, pENTR-Flag-MYPT1 D1 lacking aa 11–286, pENTR-Flag-MYPT1 D2 lacking aa 287–514, pENTR-Flag-MYPT1 D3 lacking aa 515–799 or pENTR-Flag-MYPT1 D4 lacking aa 800–1020 were generated by PCR using pENTR-MYPT1 as a template. An *Escherichia coli* expression vector for GST-MYPT1 was constructed using the expression vector, pGEX5X-1 (Pharmacia) and cDNA encoding MYPT1 protein. Expression plasmids for mutated NUAK2 and mutated MYPT1 were generated using the QuickChange site-directed mutagenesis kit (Stratagene) following the manufacturer's instructions. All constructs were verified by sequencing.

Co-immunoprecipitation assay. HEK293T cells were transfected with 5 μg cDNA/60 mm dish using Lipofectamine 2000. Two days after transfection, cells were lysed in lysis buffer (1% Nonidet P-40, 0.15 M NaCl, 20 mM Tris, pH 7.2, and 2 mM EDTA including protease inhibitor cocktail (Nacalai)). We then incubated with anti-V5, anti-Myc or anti-Flag agarose for 1 h at 4 °C. After extensive washing, immunoprecipitated samples were subjected to SDS–PAGE and immunoblotting was performed as described previously [7].

In vitro kinase assay. The following recombinant proteins were purchased: human NUAK2 (Cell Signaling), and ROCK-II, human active (Upstate Biotechnology). Bacterially purified glutathione S-transferase (GST) fusing proteins were used as substrates. Recombinant proteins were equilibrated in kinase buffer [0.15 M NaCl, 20 mM MOPS (pH 7.0), 10 μM $MgCl_2$, 10% glycerol, and 1 mM DTT], and then incubated with 10 μCi of [γ-^{32} P] ATP (Amersham) and substrates at 30 °C for 60 min. Each sample was boiled in SDS sample buffer for 3 min, and eluted proteins were analyzed by SDS–PAGE. The gel was dried and autoradiographed. ROCK-II, human active (0.317 pmol) and NUAK2 (1.33 pmol) were used in this assay.

Identification of a NUAK2-binding protein (p130). We used HEK293T cells expressing pcDNA3.1-Flag-tagged-NUAK2, lysed them with 1 ml of lysis buffer and immunoprecipitated them with anti-Flag antibody followed by elution with Flag peptide (100 μg/ml). An in vitro kinase assay was performed with the eluate in the presence of [γ-^{32}P] ATP followed by SDS–PAGE, and the radioactivity was detected by a BAS imaging analyzer (Fuji). The FLAG peptide eluate was injected onto a phenyl-reverse phase—HPLC column (4.6 × 250 mm, Nacalai) equilibrated with 0.1% trifluoroacetic acid and 5% acetonitrile. Fractions were eluted with a linear gradient of 35–45% acetonitrile at a flow rate of 1 ml/min. Each fraction was lyophilized and separated by SDS–PAGE. Radioactivity was detected by BAS imaging system.

Data analysis. Statistical significance was assessed with ANOVA using the Fisher's post hoc test. A value of $p < 0.05$ was considered to be statistically significant.

Table 1
Expression levels and fold change of the upregulated genes by TNFα in HUVECs (top 20)

Gene name	Accession No.	Control group	TNFα group	Fold change (TNFα/Control)
CCL20	NM_004591.1	0.04	7.33	168.20
E-selectin	NM_000450.1	0.08	5.11	70.63
IL-8	NM_000584.1	0.16	8.16	50.35
Coagulation factor III	NM_001993.2	0.29	7.17	24.96
TNFAIP3	NM_006290.1	0.21	4.08	19.05
VCAM1	NM_001078.1	0.16	3.03	18.95
CXCL3	NM_002090.1	0.27	5.07	18.46
CXCL2	NM_002089	0.34	4.99	14.68
TNFAIP2	NM_006291.1	0.26	3.55	13.52
CXCL1	NM_001511.1	0.32	3.70	11.70
CXCR7	NM_020311	0.37	4.02	10.77
ICAM1	NM_000201.1	0.23	2.36	10.34
TNFAIP8	NM_014350.1	0.50	5.01	9.95
Ephrin-A1	NM_004428.1	0.26	2.24	8.63
CD69 antigen	NM_001781.1	0.53	3.93	7.43
CX3CL1	NM_002996	0.36	2.46	6.75
RND1	NM_014470	0.32	2.04	6.37
PMAIP1	NM_021127.1	0.73	4.58	6.26
NUAK2	NM_030952.1	0.31	1.91	6.24
CCL2	NM_002982	0.42	2.47	5.87

HUVECs were stimulated with TNFα (20 ng/ml) (TNFα group) or medium only (Control) for 2 h. Every time, a pair of TNFα and Control was used for cDNA microarray examination, which was repeated for three times in different date. Data are mean for the three times. Only the genes that were upregulated by TNFα for more than 3-folds every times were included in this table. The expression levels were normalized intensity (linear scale).

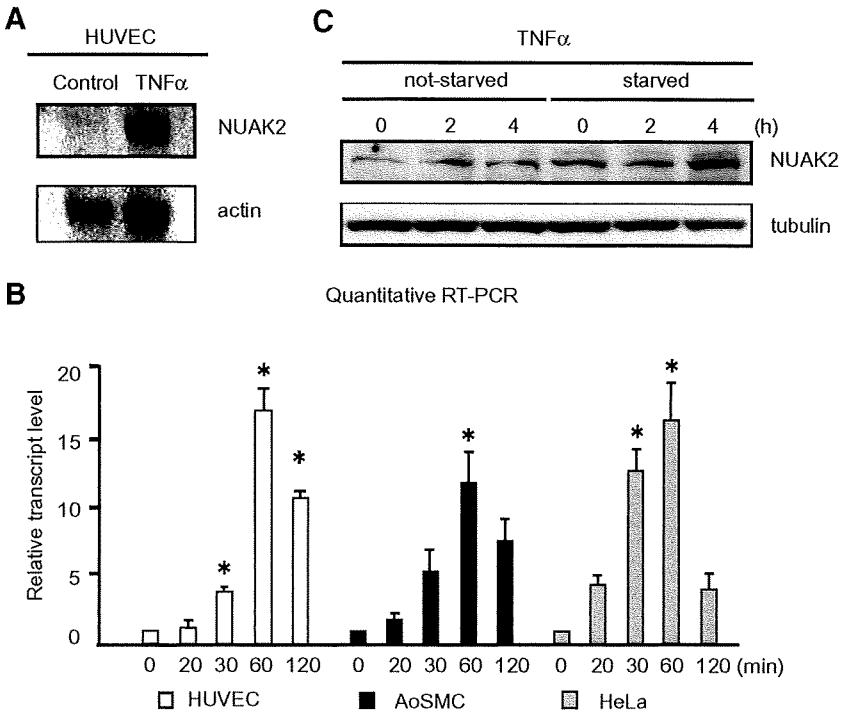

Fig. 1. TNFα induces upregulation of human NUAK2 expression. (A) Northern blot analysis. HUVECs were treated with TNFα (20 ng/ml) for 2 h or control. Total RNA was harvested, electrophoresed, and blotted to the nitrocellulose membrane. The membrane was probed with cDNA for human NUAK2. Beta actin was used as an internal control for mRNA loading. (B) Time course of NUAK2 mRNA levels. Various cell lines were treated with TNFα (20 ng/ml) for the indicated times. Each sample was analyzed in duplicate and experiments were performed in triplicate. (C) HeLa cells were either not starved or starved for 18 h in DMEM containing 0.5% serum. Starved and unstarved cells were then treated with TNFα (20 ng/ml) for indicated times. Cells were lysed and immunoblotting was performed with the indicated antibodies. For panels B, error bars represent SEM. $^{*}P < 0.05$ versus baseline.

Results

TNFα induced NUAK2 mRNA and protein expressions

To identify the specific expression targets of TNFα, the profiles of mRNA expression extracted from HUVECs were analyzed. Triplicate assay of gene chip revealed that 57 genes were enhanced their expressions 2 h after TNFα treatment. Most of these genes increased more than 3-folds are chemokines and their related molecules such as their receptors, adhesion molecules, and transcription factors (Table 1). Among them, one kinase, NUAK2, was greatly enhanced its expression by TNFα. No other kinases were enhanced its expression more than 3-folds, suggesting that NUAK2 is only a strongly inducible kinase by TNFα signaling in endothelial cells. This result was confirmed by Northern blot analysis (Fig. 1A). Quantitative PCR revealed that an enhanced NUAK2 expression after TNFα treatment was seen not only in HUVECs but also in other cell lines in a time-dependent manner (Fig. 1B). Increasing protein level by TNFα was also confirmed by immunoblotting with anti-NUAK2 antibody (Fig. 1C).

NUAK2-associated kinase activity

Since the substrate for NUAK2 has not been identified, we screened a protein which bound to NUAK2 and was phosphorylated by NUAK2. We employed a kinase-dead construct of NUAK2 (Flag-KD-NUAK2) in which Lys81 was replaced with Arg as a control. HEK293T cells were transiently transfected with Flag-WT-NUAK2 or Flag-KD-NUAK2. Immunoprecipitation assay was performed with whole-cell extracts using anti-Flag antibody followed by elution with Flag peptide. An in vitro kinase assay was performed with the eluate in the presence of [γ-^{32}P] ATP. NUAK2 was autophosphorylated in vitro [4]. Besides NUAK2 radioactivity, a phosphorylated band at the size of 130 kDa (p130) was co-immunoprecipitated

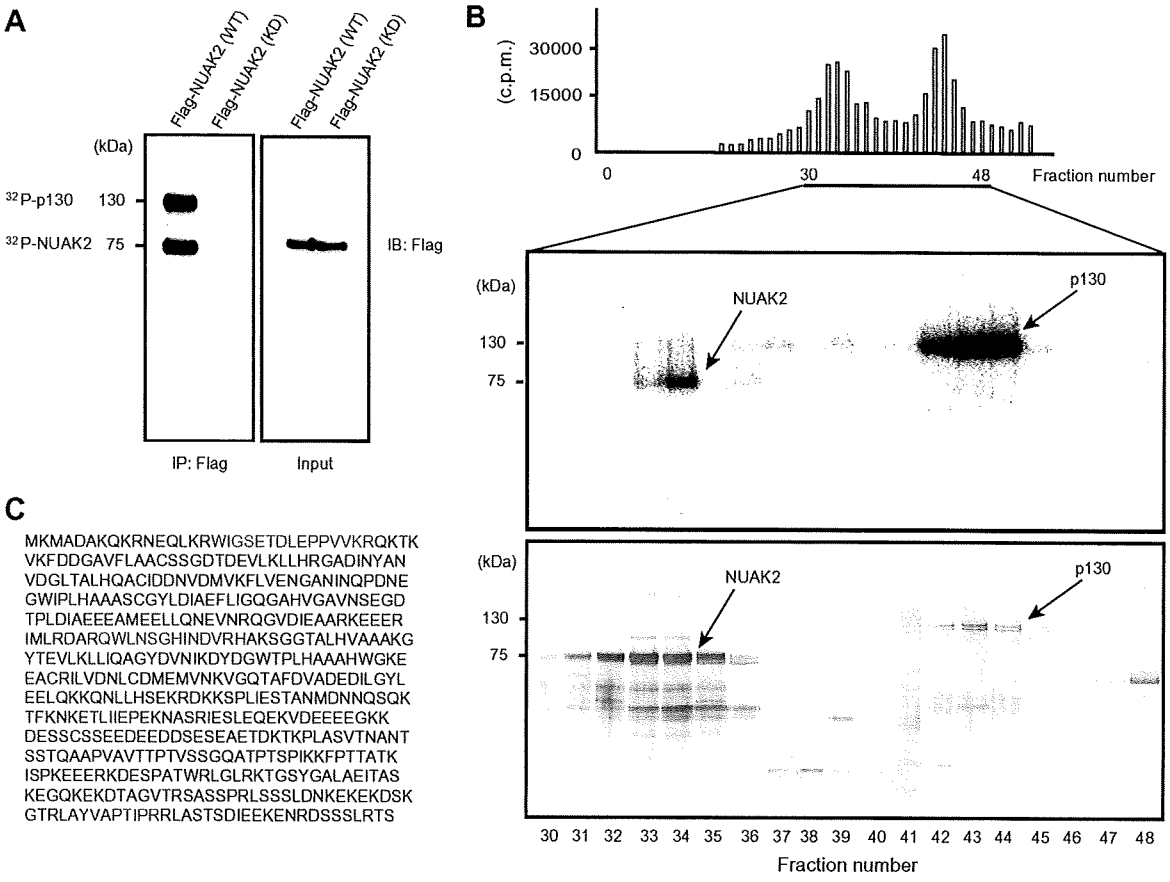

Fig. 2. Purification and identification of MYPT1. (A) HEK293T cells were transiently transfected with Flag-WT-NUAK2 or Flag-KD-NUAK2. Immunoprecipitation assay was performed with whole-cell extracts using anti-Flag antibody followed by elution with Flag peptide. An in vitro kinase assay was performed with the eluate in the presence of [γ-^{32}P] ATP (left panel). The lysates were immunoblotted with anti-Flag antibody (right panel). (B) The complex of radiolabeled NUAK2 and p130 was separated by a phenyl reverse-phase column and indicated fractions were quantified for phosphorylation of the complex (upper panel). These proteins in the indicated fractions were resolved by SDS–PAGE followed by autoradiography (middle panel). Large-scale purification of the protein complex was done using the same protocol without radioactive material. The purified products of the protein complex were resolved on SDS–PAGE and silver stained (lower panel). (C) Amino acid sequence of human MYPT1. The peptides derived from the purified protein (p130), which fitted with those of human MYPT1 as assessed by mass spectrometry, are shown in bold red. (For interpretation of the references to color in this figure legend, the reader is referred to the web version of this article.)

(Fig. 2A). In the control lane, neither NUAK2 nor p130 could be detected, suggesting that p130 was a NUAK2-binding substrate.

Purification of NUAK2 substrate

To characterize p130, we applied the Flag eluate to a reverse phase column. There were two radioactive peaks (fraction numbers 32–34, 42–44) detected in these fractions (Fig. 2B, upper panel) and each fraction was electrophoresed followed by autoradiography (Fig. 2B, middle panel). NUAK2 and p130 were well separated and matched to radioactive peak. To identify p130, we scaled up the purification procedure using HEK293T cells (4.0×10^7) expressing Flag-tagged NUAK2 without radioactive material. The purified products of the protein complex were resolved by SDS–PAGE and silver stained. Silver staining of these fractions detected NUAK2 and p130 (Fig. 2B, lower panel). We analyzed the peptides digested from the p130 band by mass spectrometry. P130 included fragments of the amino acid sequences of WIGSETDLEPPVVKR, QWLNSGHINDVR and LAYVAPTIPR that matched human myosin phosphatase targeting subunit 1 (MYPT1) (Fig. 2C).

MYPT1 is associated with NUAK2

To test whether MYPT1 is associated with NUAK2, HEK293T cells were transiently transfected with or without Myc-NUAK2. Protein extracts were subjected to immunoprecipitation with anti-Myc antibody, followed by immunoblotting with anti-MYPT1 antibody. We confirmed direct binding of endogenous MYPT1 to recombinant NUAK2 (Fig. 3A). Next, to identify the binding site on MYPT1 for NUAK2, we constructed several MYPT1 deletion mutants (Fig. 3B). Mutation analysis revealed that the NUAK2-binding domain corresponded to the C-terminal domain (amino acids 800–1020) of MYPT1 (Fig. 3C).

In vitro phosphorylation of MYPT1 by NUAK2

Recombinant human NUAK2 purified by baculovirus expression system efficiently phosphorylated *E. coli* recombinant MYPT1, suggesting that NUAK2 directly phosphorylates MYPT1 (Fig. 4A). Rho-kinase (ROCK) is

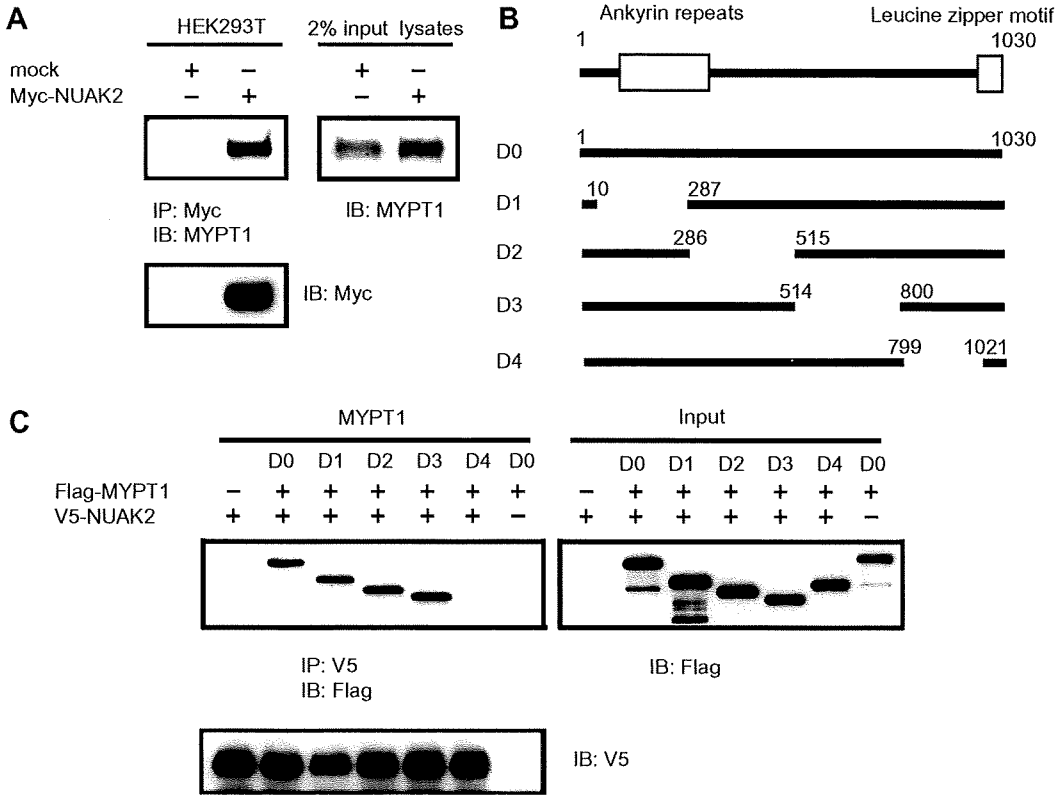

Fig. 3. NUAK2 interacts with MYPT1. (A) HEK293T cells were transiently transfected with mock or Myc-tagged NUAK2. Whole-cell extracts were subjected to immunoprecipitation assays using anti-Myc antibody followed by immunoblotting using anti-MYPT1 antibody. The same filter was reprobed with anti-Myc antibody. The same lysates were also analyzed by immunoblotting using anti-MYPT1 antibody. (B) Schematic model of the MYPT1 deletion mutants. The numbers are the amino acid number. (C) HEK293T cells were transiently transfected with V5-tagged NUAK2, Flag-tagged WT or various truncated MYPT1, alone, or together as indicated. Co-immunoprecipitation assays were performed with whole-cell extracts using anti-V5 antibody, followed by immunoblotting using anti-V5 or anti-Flag antibodies. The same lysates were also analyzed by immunoblotting using anti-Flag antibody.

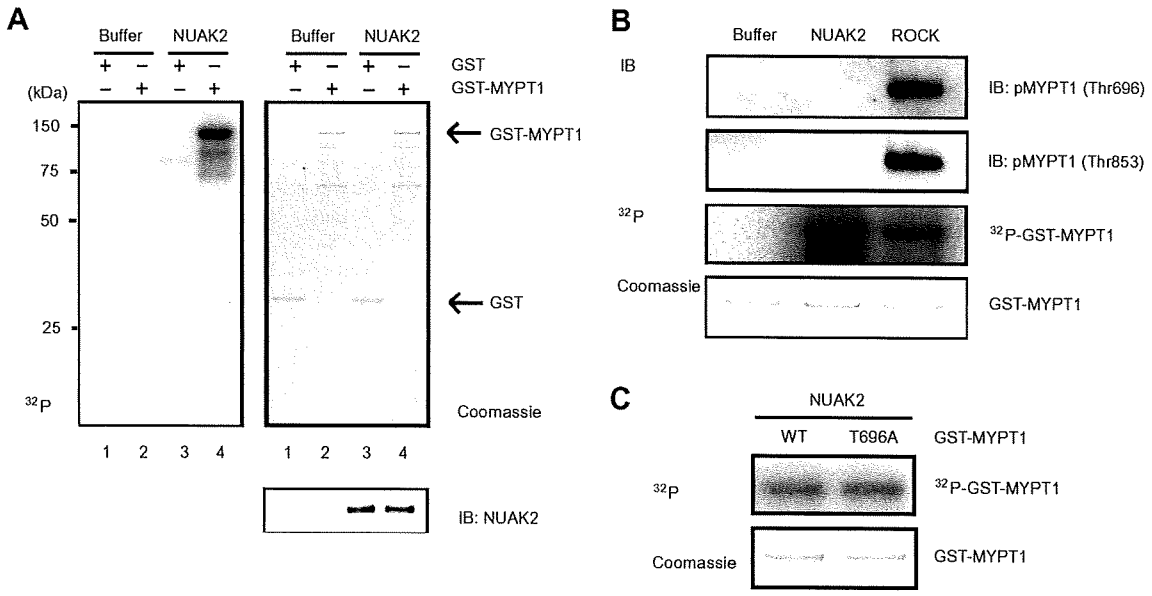

Fig. 4. NUAK2 phosphorylates MYPT1 at another site(s), other than known ROCK phosphorylation sites. (A) GST-alone (lanes 1 and 3) or GST-MYPT1 (lanes 2 and 4) were subjected to an in vitro kinase assay with control (lanes 1 and 2) or GST-NUAK2 (lanes 3 and 4), followed by autoradiography (left panel); Coomassie stain of the same gel (right upper panel), or by immunoblotting with anti-NUAK2 antibody (right lower panel). (B) GST-MYPT1 phosphorylated by recombinant NUAK2 or ROCK was resolved by SDS–PAGE followed by immunoblotting with anti-phosphospecific antibodies against MYPT1 (Thr696 or Thr853), or by autoradiography, or by Coomassie stain, as indicated. These results are representative of three independent experiments. (C) WT or the T696A mutant form of GST-MYPT1 phosphorylated by GST-NUAK2 was resolved by SDS–PAGE followed by autoradiography (upper panel); Coomassie stain of the same gel (lower panel).

known to the major kinase responsible for phosphorylation of MYPT1 [8]. To investigate how the MYPT1 phosphorylation by NUAK2 was regulated, we compared MYPT1 phosphorylation by NUAK2 and that by ROCK. ROCK is known to phosphorylate Thr696 and Thr853 in MYPT1. ROCK phosphorylated MYPT1 at the Thr696 and Thr853, confirmed by immunoblotting with anti-phospho-specific antibodies. Surprisingly, however, NUAK2 did not enhance the phosphorylation of either Thr696 or Thr853 (Fig. 4B). The non-phosphorylatable T696A mutant MYPT1 in which Thr696 was replaced with Ala was phosphorylated by NUAK2 to the same extent as WT-MYPT1 (Fig. 4C). Similarly, the T853A mutant MYPT1 also was phosphorylated by NUAK2 to the same extent as WT-MYPT1 (data not shown). These data suggests that NUAK2 phosphorylates MYPT1 at another site(s), other than known ROCK phosphorylation sites.

Discussion

TNFα is a pleiotropic cytokine that mediates diverse biological responses. To investigate the signal transduction pathways modulated by TNFα and their effect on endothelial cells, the profiles of mRNA expression extracted from HUVECs were analyzed. Most of TNFα-induced genes were chemokine family molecules and chemokine related molecules. We focused on one kinase, NUAK2 among them because it was strongly induced by TNFα. However, none of its substrate has been reported. Knowledge of kinase-substrate relationships is essential to dissect the signaling and regulatory events in which each kinase participates [9]. Direct binding of kinase to its substrate is often reported. Structural analysis reveals that the several binding sites besides catalytic site exist between kinase and its substrate [10]. The kinetics of reactions needs to be enhanced by binding between substrate and kinase. Those affinities might help efficient purification of substrate for target kinase. We successfully purified MYPT1 as a novel substrate for NUAK2 with simple two-step purification. This method is useful for rapid identification of an unknown substrate for certain kinase and can be applied for other substrate screening of kinases.

MYPT1 is a regulatory subunit of myosin phosphatase (MP) which catalyzes dephosphorylation of MLC. Phosphorylation of myosin light chain (MLC) elicits many cellular functions, including smooth muscle contraction [11,12]. MP activity is known to be regulated by upstream kinases. ROCK is most intensively examined [8]. ROCK directly binds MYPT1 and phosphorylates Thr696 and Thr853 of MYPT1 [13]. Phosphorylated MYPT1 by ROCK reduced MP activity resulting increased phosphorylation of MLC [14]. Several other kinases (MYPT1 kinase, integrin-linked kinase and myotonic dystrophy protein kinase) also can phosphorylate the same inhibitory site (Thr696) on MYPT1 [15–17]. The mechanism to reduce MP activity by MYPT1 phosphorylation is still unknown, however, phosphorylation of Thr853 was suggested to directly reduce MYPT1 binding to myosin [18]. Dissociation of the MP holoenzyme by MYPT1 phosphorylation is another suggested mechanism of reduced MYPT1 activ-

ity [19]. NUAK2 did not phosphorylate MYPT1 at either Thr696 or Thr853, confirmed by immunoblotting with anti-phosphospecific antibodies (Fig. 4B) and mutation analysis of MYPT1 (Fig. 4C). These data suggest that NUAK2 phosphorylates MYPT1 at a different site(s) to elicit different regulatory functions. Further characterization of phosphorylation site(s) and elucidation of MYPT1 regulation by NUAK2 are necessary for future study.

Physiological function has been seldom analyzed about NUAK2, however, Legembre et al. reported that NUAK2 works as a part of antiapoptotic signals and an enhancer of cell mobility [4]. If NUAK2 phosphorylates MYPT1 and modulates MLC phosphorylation, these phenotypes would be explained by functional regulation of MYPT1 and its target molecule, myosin. One intriguing thing about NUAK2 is that this is the only kinase highly induced by TNFα. Most of other induced genes were chemokines and adhesion molecules. Chemokine induces chemotaxis of various normal cells, and also plays an important role for invasiveness of tumor cells partly reflected by cell motility. NUAK2-mediated MYPT1 phosphorylation might enhance these chemokine signaling by modifying myosin motor function. In tumor cell lines, TNFα also strongly induces expression of NUAK2, which is related to its motility and invasiveness [4]. These tumor characteristics might be also regulated by NUAK2-mediated myosin motor regulation. The physiological significance of the phosphorylation of MYPT1 by NUAK2 both in normal cells and in tumor cells is now under investigation.

Acknowledgments

We thank A. Ogai, H.O. kuda, S. Ikezawa and Y. Hamada for technical assistance. We thank Dr. M. Ito for thoughtful discussion. This study was supported by a Grant from Japan Cardiovascular Research Foundation. Supported by Grants-in-aid for Human Genome, Tissue Engineering, and Food Biotechnology (H13-Genome-011) in Health and Labor Sciences Research Grants Research, Comprehensive Research on Aging and Health (H13-21 seiki (seikatsu)-23) in Health and Labor Sciences Research Grants Research from Ministry of Health and Labor and Welfare, Takeda Science Foundation and Grant-in-aid for Scientific Research (No. 17390229) from the Ministry of Education, Science, and Culture, Japan.

References

[1] T. Collins, M.A. Read, A.S. Neish, M.Z. Whitley, D. Thanos, T. Maniatis, Transcriptional regulation of endothelial cell adhesion molecules: NF-kappa B and cytokine-inducible enhancers, FASEB J. 9 (1995) 899–909.

[2] D.L. Lefebvre, Y. Bai, N. Shahmolky, M. Sharma, R. Poon, D.J. Drucker, C.F. Rosen, Identification and characterization of a novel sucrose-non-fermenting protein kinase/AMP-activated protein kinase-related protein kinase, SNARK, Biochem. J. 355 (2001) 297–305.

[3] D.L. Lefebvre, C.F. Rosen, Regulation of SNARK activity in response to cellular stresses, Biochim. Biophys. Acta 1724 (2005) 71–85.

[4] P. Legembre, R. Schickel, B.C. Barnhart, M.E. Peter, Identification of SNF1/AMP kinase-related kinase as an NF-kappaB-regulated anti-apoptotic kinase involved in CD95-induced motility and invasiveness, J. Biol. Chem. 279 (2004) 46742–46747.

[5] Y. Asano, S. Takashima, M. Asakura, Y. Shintani, Y. Liao, T. Minamino, H. Asanuma, S. Sanada, J. Kim, A. Ogai, T. Fukushima, Y. Oikawa, Y. Okazaki, Y. Kaneda, M. Sato, J. Miyazaki, S. Kitamura, H. Tomoike, M. Kitakaze, M. Hori, Lamr1 functional retroposon causes right ventricular dysplasia in mice, Nat. Genet. 36 (2004) 123–130.

[6] S. Soker, S. Takashima, H.Q. Miao, G. Neufeld, M. Klagsbrun, Neuropilin-1 is expressed by endothelial and tumor cells as an isoform-specific receptor for vascular endothelial growth factor, Cell 92 (1998) 735–745.

[7] T. Minamino, V. Gaussin, F.J. DeMayo, M.D. Schneider, Inducible gene targeting in postnatal myocardium by cardiac-specific expression of a hormone-activated Cre fusion protein, Circ. Res. 88 (2001) 587–592.

[8] K. Kimura, M. Ito, M. Amano, K. Chihara, Y. Fukata, M. Nakafuku, B. Yamamori, J. Feng, T. Nakano, K. Okawa, A. Iwamatsu, K. Kaibuchi, Regulation of myosin phosphatase by Rho and Rho-associated kinase (Rho-kinase), Science 273 (1996) 245–248.

[9] D.C. Berwick, J.M. Tavare, Identifying protein kinase substrates: hunting for the organ-grinder's monkeys, Trends Biochem. Sci. 29 (2004) 227–232.

[10] C. Kim, N.H. Xuong, S.S. Taylor, Crystal structure of a complex between the catalytic and regulatory (RIalpha) subunits of PKA, Science 307 (2005) 690–696.

[11] F. Matsumura, Regulation of myosin II during cytokinesis in higher eukaryotes, Trends Cell Biol. 15 (2005) 371–377.

[12] M. Ito, T. Nakano, F. Erdodi, D.J. Hartshorne, Myosin phosphatase: structure, regulation and function, Mol. Cell Biochem. 259 (2004) 197–209.

[13] D. Johnson, P. Cohen, M.X. Chen, Y.H. Chen, P.T. Cohen, Identification of the regions on the M110 subunit of protein phosphatase 1 M that interact with the M21 subunit and with myosin, Eur. J. Biochem. 244 (1997) 931–939.

[14] J. Feng, M. Ito, K. Ichikawa, N. Isaka, M. Nishikawa, D.J. Hartshorne, T. Nakano, Inhibitory phosphorylation site for Rho-associated kinase on smooth muscle myosin phosphatase, J. Biol. Chem. 274 (1999) 37385–37390.

[15] J.A. MacDonald, M.A. Borman, A. Muranyi, A.V. Somlyo, D.J. Hartshorne, T.A. Haystead, Identification of the endogenous smooth muscle myosin phosphatase-associated kinase, Proc. Natl. Acad. Sci. USA 98 (2001) 2419–2424.

[16] A. Muranyi, J.A. MacDonald, J.T. Deng, D.P. Wilson, T.A. Haystead, M.P. Walsh, F. Erdodi, E. Kiss, Y. Wu, D.J. Hartshorne, Phosphorylation of the myosin phosphatase target subunit by integrin-linked kinase, Biochem. J. 366 (2002) 211–216.

[17] A. Muranyi, R. Zhang, F. Liu, K. Hirano, M. Ito, H.F. Epstein, D.J. Hartshorne, Myotonic dystrophy protein kinase phosphorylates the myosin phosphatase targeting subunit and inhibits myosin phosphatase activity, FEBS Lett. 493 (2001) 80–84.

[18] G. Velasco, C. Armstrong, N. Morrice, S. Frame, P. Cohen, Phosphorylation of the regulatory subunit of smooth muscle protein phosphatase 1 M at Thr850 induces its dissociation from myosin, FEBS Lett. 527 (2002) 101–104.

[19] J. Tanaka, M. Ito, J. Feng, K. Ichikawa, T. Hamaguchi, M. Nakamura, D.J. Hartshorne, T. Nakano, Interaction of myosin phosphatase target subunit 1 with the catalytic subunit of type 1 protein phosphatase, Biochemistry 37 (1998) 16697–16703.